Stem Cell Reports
Article
ISSCR
OPEN ACCESS

ALDH-Dependent Glycolytic Activation Mediates Stemness and Paclitaxel Resistance in Patient-Derived Spheroid Models of Uterine Endometrial Cancer

Yutaro Mori,[1] Kaoru Yamawaki,[1] Tatsuya Ishiguro,[1,*] Kosuke Yoshihara,[1] Haruka Ueda,[1] Ai Sato,[2] Hirokazu Ohata,[2] Yohko Yoshida,[3] Tohru Minamino,[3] Koji Okamoto,[2] and Takayuki Enomoto[1,*]
[1]Department of Obstetrics and Gynecology, Niigata University Graduate School of Medical and Dental Sciences, 1-757 Asahimachi-dori, Niigata, Niigata 951-8510, Japan
[2]Division of Cancer Differentiation, National Cancer Center Research Institute, 5-1-1 Tsukiji, Chuo-ku, Tokyo 104-0045, Japan
[3]Department of Cardiovascular Biology and Medicine, Niigata University Graduate School of Medical and Dental Sciences, 1-757 Asahimachi-dori, Niigata, Niigata 951-8510, Japan
*Correspondence: tishigur@med.niigata-u.ac.jp (T.I.), enomoto@med.niigata-u.ac.jp (T.E.)
https://doi.org/10.1016/j.stemcr.2019.08.015

SUMMARY

Uterine endometrial cancer is associated with poor survival outcomes in patients with advanced-stage disease. Here, we developed a three-dimensional cell cultivation method of endometrioid cancer stem-like cells with high aldehyde dehydrogenase (ALDH) activity from clinical specimens. ALDH inhibition synergized with paclitaxel to block cancer proliferation. In the clinical setting, high ALDH1A1 expression was associated with poor survival. A high level of ALDH correlated with an increase of glucose uptake, activation of the glycolytic pathway, and elevation of glucose transporter 1 (GLUT1). Blockade of GLUT1 inhibited characteristics of cancer stem cells. Similarly to ALDH inhibition, GLUT1 inhibition synergized with paclitaxel to block endometrial cancer proliferation. Our data indicated that ALDH-dependent GLUT1 activation and the resulting glycolytic activation are of clinical importance for both prognostic evaluation and therapeutic decision-making in endometrial cancer patients. In addition, the synergistic effects of taxane compounds and ALDH or GLUT1 inhibitors may serve as a new clinical treatment option for endometrial cancer.

INTRODUCTION

Uterine endometrial cancer is one of the most common gynecological malignancies (Morice et al., 2016). Despite macroscopic complete surgical resection of the cancerous tumor plus adjuvant chemotherapy, high-grade endometrial cancer cells tend to form recurrent metastatic tumors (Nomura et al., 2011; Siegel et al., 2015). Moreover, the 5-year overall survival rate for advanced-stage cancer with distance metastasis is no more than ~25% (Aoki, 2014). Currently combination drug therapies with taxanes (paclitaxel or docetaxel) and platinum analogs (carboplatin or cisplatin) are used as a first-line chemotherapy for endometrial cancer (Bestvina and Fleming, 2016; Nomura et al., 2011); however, the appropriate chemotherapy regimen for high-risk disease is still controversial (de Boer et al., 2018; Morice et al., 2016). Thus, establishing a better chemotherapeutic strategy is essential for the treatment of advanced endometrial cancer.

Cancer stem cells (CSCs) are a small fraction of cancer cells with central roles in cancer propagation and proliferation among heterogeneous tumors (Lytle et al., 2018) and are thought to contribute to metastatic spread and resistance to chemotherapy and radiotherapy. Previous research has shown that a small population of freshly isolated cells from clinical endometrial cancer tissues has the capacity for clonogenicity *in vitro* and tumorigenicity *in vivo* (Hubbard et al., 2009), and that transiently cultured endometrial cells are resistant to cisplatin- and paclitaxel-induced cytotoxicity (Rutella et al., 2009), suggesting the presence of CSC-like cells in endometrial cancers. However, the detailed biology of endometrial CSCs in clinical specimens has not been elucidated, potentially as a result of difficulties in the stable *in vitro* cultivation of endometrial CSCs isolated from clinical tumors.

Cells with characteristics of CSCs can be expanded *in vitro* under floating conditions in a unique three-dimensional format called tumor-derived spheroids or tumor spheres (Pastrana et al., 2011; Valent et al., 2012); the spheroid cultivation system may facilitate identification of the biological characteristics of CSCs. Hence, this cultivation method has been established in several types of malignant tumors (Dontu et al., 2003; Lonardo et al., 2011; Ricci-Vitiani et al., 2007; Singh et al., 2003). Previously, we generated stable cancer spheroid cells with CSC characteristics from clinical colorectal and ovarian cancer specimens (Ohata et al., 2012; Ishiguro et al., 2016).

In this study, we aimed to develop a stable culture method for CSC spheroids from clinical endometrial cancer specimens. Our results demonstrated that aldehyde dehydrogenase (ALDH), via enhanced glycolysis through glucose transporter 1 (GLUT1) upregulation, plays an important role in the maintenance of endometrial CSCs. Further investigation revealed the synergistic effects of

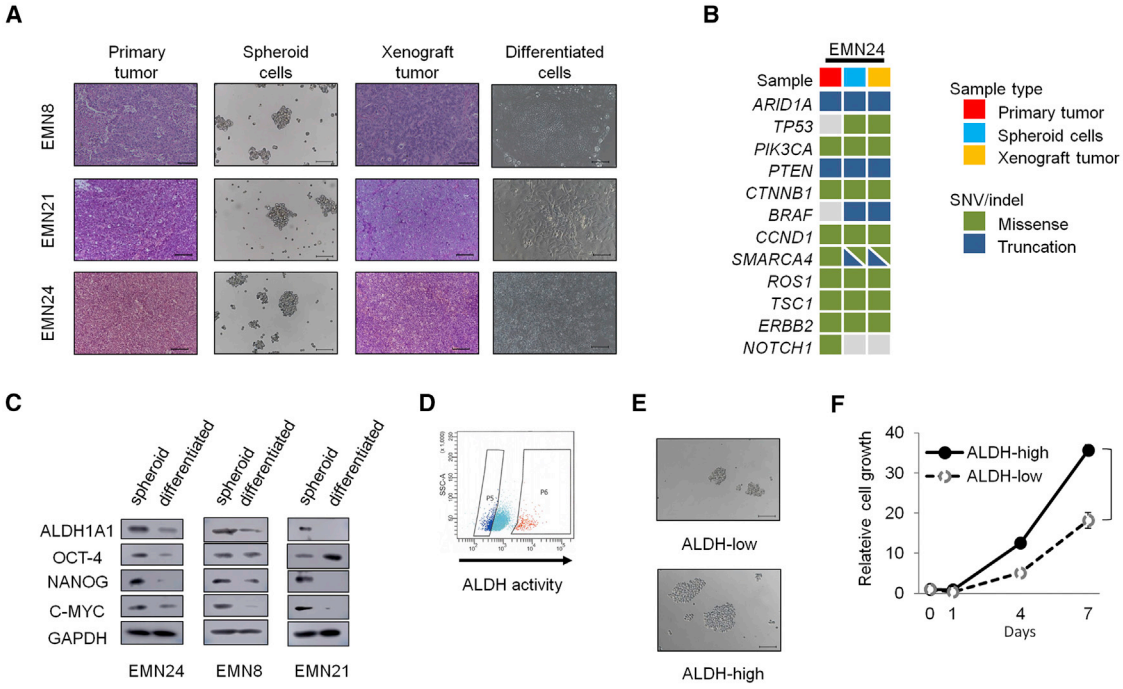

(legend on next page)

inhibition of ALDH activity or GLUT1 with taxane treatment on cell proliferation *in vitro* and tumorigenesis *in vivo*.

RESULTS

Human Uterine Endometrial Cancer Spheroid Cells Exhibit CSC-like Characteristics

To develop new therapeutic strategies for refractory endometrial cancer, *in vitro* three-dimensional culture systems from human clinical specimens may provide a useful platform. Hence, we attempted to establish a cultivation method for spheroid cells from human uterine endometrial cancer tumors. Spheroid cells from 8 of 19 high-grade carcinoma samples (42%), and one case of grade 2 endometrioid carcinoma could be expanded under the spheroid culture conditions (Table S1; Figure 1A). Interestingly, the established endometrial cancer spheroid cells were capable of proliferating under floating conditions in the absence of ROCK inhibitors, which were required for proliferation and maintenance of ovarian and colorectal cancer spheroid cells (Ishiguro et al., 2016; Ohata et al., 2012).

To evaluate the tumorigenicity of these spheroid cells, cells were injected into immunodeficient NOG mice. The generated xenograft tumors were histologically similar to the original human endometrial tumors (Figures 1A and S1A). Immunostaining patterns for PAX8, cytokeratin 7, and p53 were similar between primary and xenograft tumors (Figure S1B). To determine whether spheroid cells and primary tumors were genetically identical, targeted sequencing analysis was performed for 114 cancer-related genes (Table S2). Overall the mutational profile of spheroid cells was identical to that of the original tumor except some mutations observed only in spheroids (Figures 1B and S1C). The mutation profiles of spheroids and xenograft are identical, indicating that xenograft formation did not significantly promote additional oncogenic mutations. Most shared mutations were previously reported as common genomic alterations in endometrial cancer tissues, i.e., *PTEN*, *PIK3CA*, *ARID1A*, and *TP53* (The Cancer Genome Atlas Network, 2013; Soumerai et al., 2018).

ALDH Activity Is Related to the CSC Characteristics of Endometrial Cancer Spheroid Cells

Next, we examined the CSC characteristics of these established spheroids. Expression levels of stemness-related markers, including Nanog, c-myc, and ALDH1A1, were higher in the spheroid cells than in differentiated cells (Figures 1A and 1C). In accordance with elevated levels of ALDH1A1, fluorescence-assisted cell sorting (FACS)-sorted spheroid cells with high ALDH activity (ALDH-high cells) could form and expand spheroids more rapidly *in vitro* than cells with no or low ALDH activity (ALDH-low cells; Figures 1D–1F and S1D–S1F). Western blot analysis showed that ALDH-high cells expressed higher levels of the stemness markers Oct-4, c-myc, and ALDH1A1 than ALDH-low cells (Figures 1G and S1G). Moreover, gene set enrichment analysis (GSEA) demonstrated that ALDH-high cells preferentially expressed stem cell-related genes found in breast cancer (false discovery rate [FDR] q value < 0.01, normalized enrichment

Figure 1. Spheroid Cells Derived from Human Endometrial Cancer with High ALDH Activity Shows CSC Characteristics and Genetic Background Similar to that of the Primary Tumor

(A) H&E staining of the primary tumor (left), bright-phase image of the indicated spheroids (center left), H&E staining of xenograft tumors (center right), bright-phase image of cells grown under differentiation conditions (right). Scale bars, 100 μm.

(B) Targeted sequencing analyses of the primary tumor, spheroid cells, and spheroid-derived xenograft tumors.

(C) Western blot analyses of the spheroid cells and differentiated cells shown in (A).

(D) FACS analyses of ALDH activity after ALDEFLUOR staining. Left gated population, ALDH-low cells; right gated population, ALDH-high cells.

(E) Bright-phase images of spheroid formation (7 days after *in vitro* cultivation). Scale bars, 100 μm.

(F) Time course analyses of cell growth in ALDH-high and ALDH-low cells after sorting. n = 4 independent experiments, $p < 0.001$, Student's t tests.

(G) Western blot analyses of ALDH-high and ALDH-low cells after sorting.

(H) Gene set enrichment analyses of gene expression profiles between ALDH-high and ALDH-low cells.

(I) Time course of ALDH activity *in vitro* after ALDEFLUOR sorting.

(J) Volume (mean ± SEM) of xenograft tumors from 1×10^5 ALDH-low and ALDH-high cells. n = 5 independent experiments, $p = 0.002$, Student's t tests.

(K) Image of mice on day 33. ALDH-low cells were injected on the left side, and ALDH-high cells were injected on the right side.

(L) H&E staining and immunostaining of xenograft tumors derived from ALDH-high and ALDH-low cells, 33 days after transplantation. Scale bars, 100 μm.

(M) Limiting dilution analysis of ALDH-high cells and ALDH-low cells *in vivo* on day 23 after subcutaneous injection. $p < 0.01$.

(N) ALDH activity after ALDEFLUOR staining in cancer cells from ALDH-high and ALDH-low xenograft tumors. Experiments in (D to G) and (I to N) were performed with EMN24 cells.

** $p < 0.01$; ***$p < 0.001$. See also Figure S1.

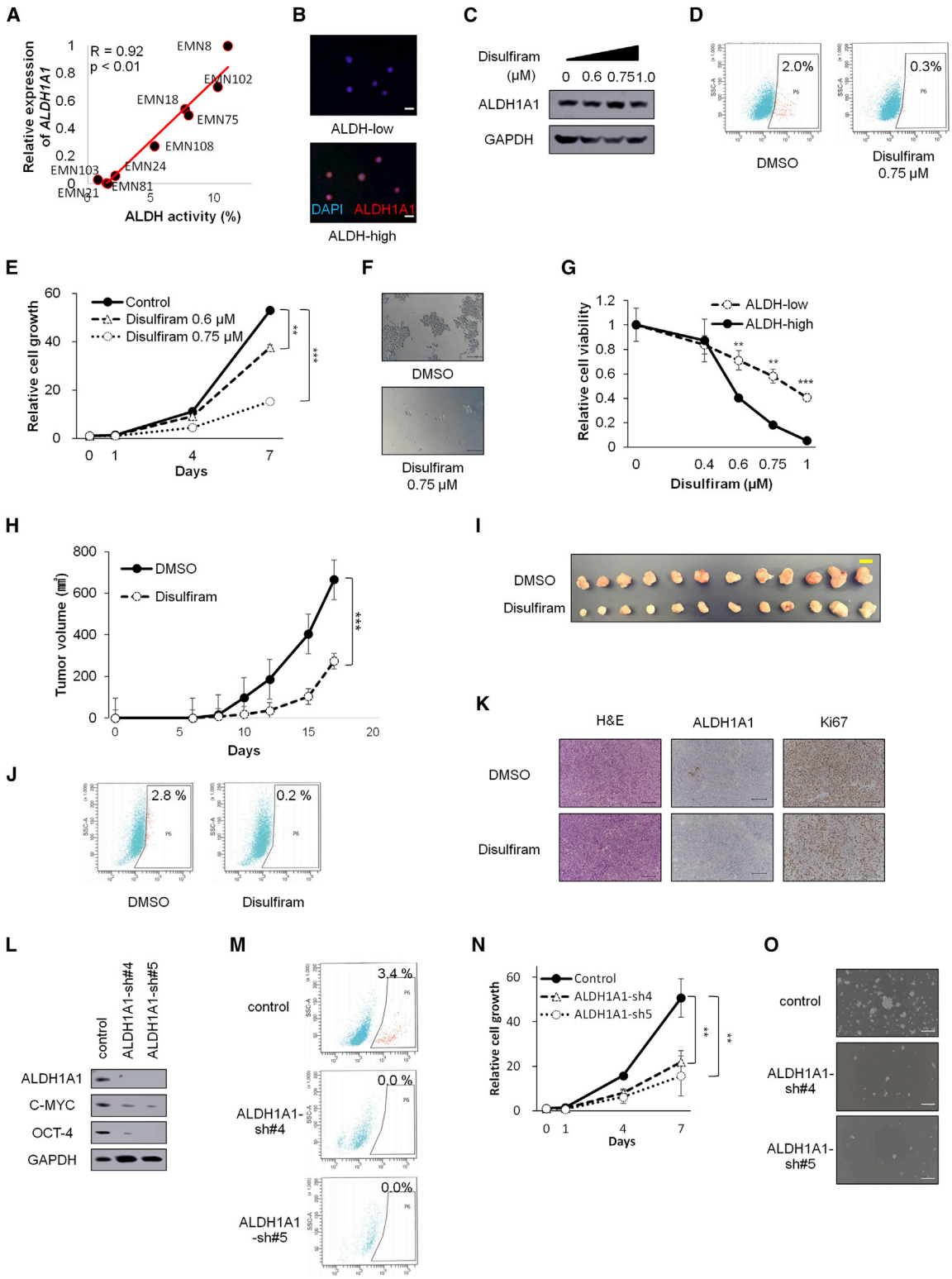

Figure 2. Inhibition of ALDH Activity Blocks the Formation and Proliferation of Spheroid Cells (EMN24 cells)

(A) Correlation between ALDH activity and *ALDH1A1* mRNA levels on culture day 10.

(B) Immunofluorescence staining with anti-ALDH1A1 antibody and DAPI in ALDH-high and ALDH-low cells after sorting. Scale bars, 20 μm.

(legend continued on next page)

score [NES] 2.16) (Pece et al., 2010) and embryonic stem cells (ESCs) (FDR q value < 0.01, NES 2.02) (Wong et al., 2008) (Figure 1H), which may reflect the activation of an ESC-like transcriptional program in endometrial cancer. Induction of stem cell-related genes was previously reported in other types of human cancers, including glioblastoma (grade 4), breast cancer, and lung cancer (Ben-Porath et al., 2008; Wong et al., 2008). Although ALDH-high cells generated both ALDH-high and ALDH-low cells, ALDH-low cells propagated more slowly than ALDH-high cells and did not give rise to ALDH-high cells during *in vitro* cultivation (Figure 1I). These results indicated that ALDH-high cells had the CSC ability to self-renew and to differentiate into ALDH-low cells. In contrast, high expression levels of CD44 or CD133 were not associated with the capability to form spheres *in vitro* (Figures S1H–S1K).

Next, we explored the tumorigenic ability of ALDH-high cells *in vivo*. The FACS-sorted ALDH-high cells generated xenograft tumors more aggressively than ALDH-low cells (Figures 1J–1L and S1L). *In vivo* serial dilution spheroid cell assays showed that the tumorigenic ability of ALDH-high cells was higher than that of ALDH-low cells ($p < 0.0001$; Figure 1M). ALDH activity assays and immunohistochemical analyses showed that the xenograft tumors from ALDH-high cells contained both ALDH-high cells and ALDH-low cells, whereas tumors from ALDH-low cells contained only ALDH-low cells (Figures 1L and 1N); these *in vivo* results were consistent with the *in vitro* results (Figure 1I). Immunohistochemical analyses also showed that xenograft tumors from ALDH-high cells contained more Ki67-positive cells than tumors from ALDH-low cells (Figure 1L). These results indicated that ALDH-low cells were derived from CSC-like ALDH-high cells.

Inhibition of ALDH Activity Reduces the Propagation of Endometrial Cancer Spheroid Cells

Next, we attempted to determine whether ALDH1A1 or other isoforms of ALDH were responsible for ALDH activity in the endometrial cancer spheroids. The ALDH family is composed of at least 19 functional isoforms with similar catalytic functions (Tomita et al., 2016). Although each of the established spheroid cells had different levels of ALDH activities, qRT-PCR analyses showed that only *ALDH1A1* mRNA expression was clearly correlated with ALDH activity (Spearman R value = 0.92, $p < 0.01$; Figures 2A and S2A). The association between ALDH1A1 expression and ALDH activity was confirmed by western blotting (Figure S2B) and by immunocytochemical analyses, which showed that most ALDH-high cells expressed detectable ALDH1A1 (Figure 2B), although some spheroid cells also expressed higher levels of other ALDH isoforms (Figure S2B).

Consistent with ALDH1A1 expression in spheroids (Figures 2A and S2B), xenograft tumors derived from EMN8 and EMN102 cells showed strong staining of ALDH1A1, whereas those from EMN103 cells showed weak expression of ALDH1A1 (Figure S2C).

We then examined differences in function after treatment with the pan-ALDH-specific inhibitor disulfiram. Although exposure to disulfiram did not significantly change ALDH1A1 expression (EMN24 cells, Figure 2C), disulfiram treatment suppressed ALDH activity (Figure 2D) and spheroid propagation (Figures 2E and 2F). Other spheroid cells (i.e., EMN81 cells) were more sensitive to disulfiram than EMN24 spheroid cells (Figures S2D–S2F), and the surviving cells retained reduced levels of ALDH1A1 expression after treatment (Figure S2G). ALDH-high cells were more sensitive to disulfiram than ALDH-low cells (Figures 2G and S2H).

(C) Western blot analyses of spheroids cells after disulfiram treatment for 24 h.
(D) FACS analyses of ALDH activity in the presence or absence of disulfiram (24 h after treatment).
(E) Time course of cell growth in spheroid cells treated with the indicated amounts of disulfiram. n = 4 independent experiments, $p < 0.001$, Student's t test.
(F) Bright-phase images of spheroids (7 days after disulfiram treatment). Scale bars, 100 μm.
(G) Responses of ALDH-high and ALDH-low cells to different concentrations of disulfiram after treatment for 7 days. n = 4 independent experiments, $p < 0.001$, Student's t test.
(H) Tumor volumes (mean ± SEM) of xenograft tumors from 1×10^5 spheroid cells subcutaneously injected. Disulfiram (40 mg/kg) was intraperitoneally injected into mice in the disulfiram-treatment group, and vehicle (DMSO) was intraperitoneally injected into mice in the control group. n = 12 independent experiments, $p < 0.001$, Student's t test.
(I) Images of whole resected tumor xenografts excised on day 17. Scale bar, 10 mm.
(J) ALDH activity of the cancer cells derived from xenograft tumors.
(K) H&E staining and immunostaining of xenograft tumors, 17 days after transplantation. Scale bars, 100 μm.
(L) Western blot analyses after infection with the indicated lentiviruses.
(M) ALDH activity in the infected cells after ALDEFLUOR staining.
(N) Time course of proliferation of infected cells. n = 4 independent experiments, $p < 0.01$, Student's t test.
(O) Bright-phase images of the infected cells on day 7. Scale bars, 100 μm.
**$p < 0.01$; ***$p < 0.001$. See also Figure S2.

To further confirm the inhibitory effects of ALDH inhibition, we used three other ALDH inhibitors, diethylaminobenzaldehyde (DEAB), CM037, and NCT501 (a selective inhibitor of ALDH1A1). Again, these ALDH inhibitors caused inhibition of ALDH activity (Figure S2I), reduction of spheroid cells (Figure S2J), and preferential cell death in ALDH-high cells (Figures S2K and S2L). Collectively, these data indicated that ALDH inhibition blocked spheroid cell propagation and spheroid formation via preferential targeting of ALDH-high cells.

Based on the effects of ALDH inhibitors on *in vitro* spheroid cells, we attempted to examine the effects of ALDH inhibitor treatment on tumor formation *in vivo*. Because disulfiram has been used in the preclinical and clinical settings (Ishiguro et al., 2016; Nechushtan et al., 2015; Safi et al., 2014; Xu et al., 2017; Yip et al., 2011), we chose disulfiram to investigate the inhibitory effects *in vivo*. Disulfiram treatment suppressed tumorigenesis in spheroid cells *in vivo* (Figures 2H and 2I), markedly reduced a fraction of ALDH-high cells in the tumor (Figure 2J), and caused decreased levels of Ki-67 staining, not ALDH1A1 staining (Figure 2K). Thus, inhibition of ALDH activity by disulfiram treatment inhibited spheroid-derived tumor growth *in vivo*.

Next, we examined the functional effects of ALDH1A1 on cancer stemness, proliferation, and ALDH activity. Inhibition of ALDH1A1 expression by shRNA lentiviral transfer caused reduction of the stemness-related markers c-myc and Oct4 (Figures 2L and S2M) and ALDH activity (Figures 2M and S2N). In addition, ALDH1A1 inhibition blocked spheroid formation and propagation *in vitro* (Figures 2N, 2O, S2O, and S2P).

Exogenous ALDH Expression Enhances the Stemness Features of Endometrial Cancer

We next examined whether exogenous ALDH1A1 overexpression enhanced the proliferation of endometrial cancer spheroid cells. Introduction of ALDH1A1 via lentivirus-mediated gene transfer into EMN24 cells augmented ALDH activity and expression of stemness-related markers (Figures 3A and 3B). Although ALDH1A1 expression caused a modest increase in the proliferation rate of the spheroids (Figures 3C and 3D), ALDH1A1 expression also resulted in the formation of the transplanted tumors that were four times larger than those formed after transplantation of control cells (Figure 3E). The xenograft tumors generated from the ALDH1A1-introduced spheroid cells contained more Ki67-positive cells than the control of xenograft tumors (Figure 3F). EMN21 cells, which showed the lowest ALDH activity among the established endometrial spheroid cells (Figure 2A), also propagated rapidly *in vitro* after the introduction of exogenous ALDH1A1 (Figures S2Q–S2T). Collectively, our data indicated that ALDH activity, which was mainly attributed to ALDH1A1 expression, played an essential role in the survival and propagation of endometrial CSCs.

Spheroid Cells with ALDH Activity Are less Sensitive to Paclitaxel

Cancer stem-like cells have been reported to be responsible for drug resistance in many cancers (Hida et al., 2017; House et al., 2017). To evaluate the drug sensitivity of cancer stem-like cells in our endometrial cancer spheroid cells, we examined the sensitivity of ALDH-high cells for paclitaxel or cisplatin, which have been used in the clinical setting as key drugs for the treatment of endometrial cancer (Nomura et al., 2011). Interestingly, although there were no significant differences in the sensitivity of ALDH-high and ALDH-low cells to cisplatin, ALDH-high cells were more resistant to paclitaxel than ALDH-low cells (Figures 4A and S3A).

Given the relative resistance of ALDH-high cells against paclitaxel, we examined whether ALDH-high cells preferentially survived following paclitaxel treatment. Treatment of spheroids with paclitaxel, but not with cisplatin, caused the proportion of ALDH-high cells to increase (Figures 4B and S3B). Consistent with the major role of ALDH1A1 in ALDH activity of spheroids, ALDH1A1 increased after exposure to paclitaxel (Figures 4C and S3C). Furthermore, evaluation of the ALDH activity and half-maximal inhibitory concentration of paclitaxel of nine established endometrial cancer spheroids revealed strong correlations (Spearman R value = 0.87, $p < 0.01$; Figure 4D). These results indicated that an ALDH-high cell population in endometrial spheroid cells was responsible for paclitaxel resistance in endometrial cancer.

Because of the relative resistance of ALDH-high cells to paclitaxel, we examined the synergistic effects of paclitaxel and an ALDH inhibitor. Disulfiram synergistically suppressed spheroid cell proliferation *in vitro* when used in combination with paclitaxel (Figures 4E–4G and S3D–S3F). Similarly, the combination of paclitaxel and other ALDH inhibitors (DEAB, CM037, and NCT501) suppressed spheroid cell propagation to a greater extent than paclitaxel alone (Figure S3G).

To determine the synergistic effects of paclitaxel and disulfiram *in vivo*, we treated spheroid cell-transplanted mice with paclitaxel with or without disulfiram. The sizes of tumors observed after combination therapy were approximately one-eighth of those after paclitaxel alone (Figures 4H and 4I). As expected, paclitaxel treatment led to an increase in the population of ALDH-high cells, which was suppressed by additional treatment with disulfiram (Figure 4J). Thus, combination therapy with paclitaxel and the ALDH inhibitor synergistically inhibited endometrial cancer cell progression in *in vivo* tumors as well as *in vitro* spheroids.

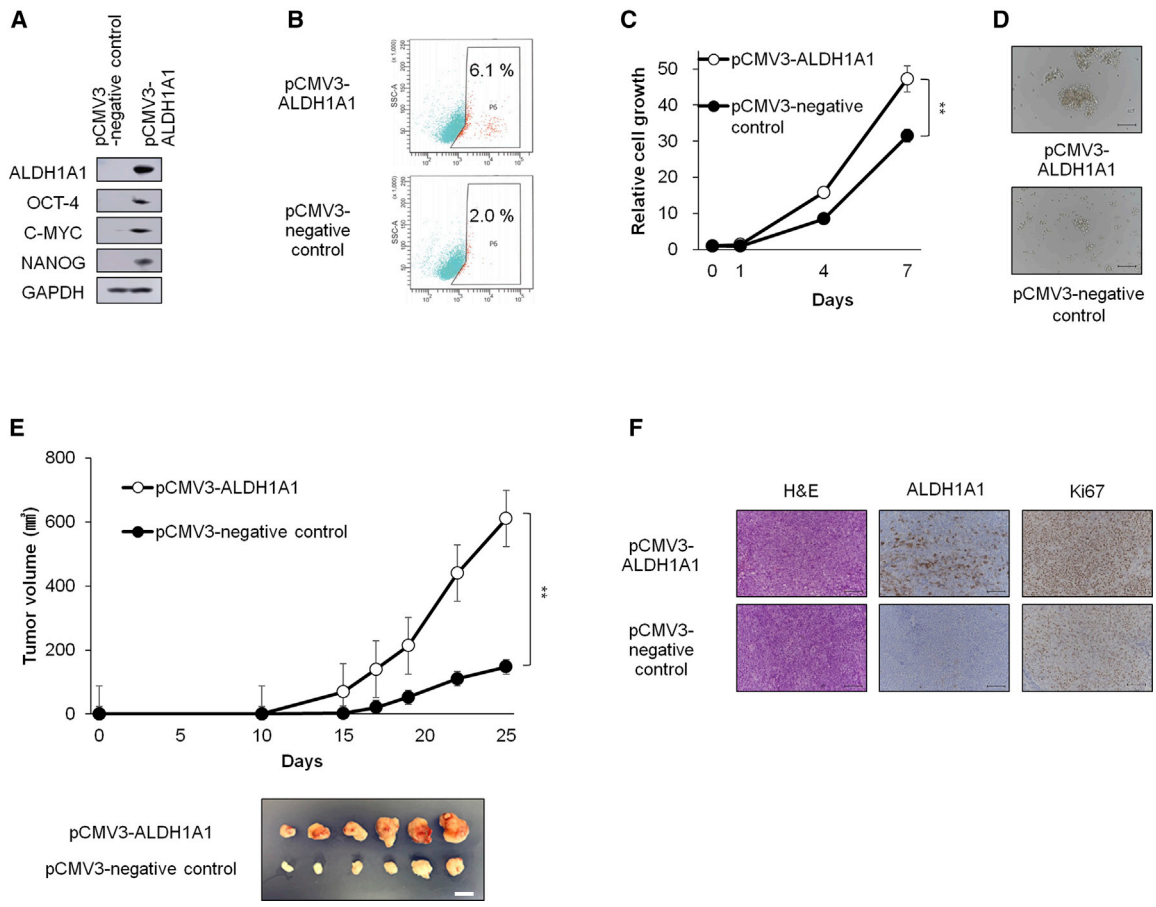

Figure 3. Exogenous ALDH1A1 Enhances the Formation and Proliferation of Spheroids and Tumorigenicity (EMN24 Cells)

(A) Western blot analyses of spheroid cells after infection with the indicated lentiviruses.

(B) ALDH activity in the infected cells after ALDEFLUOR staining.

(C) Time course of proliferation of infected cells. n = 4 independent experiments, $p < 0.01$, Student's t test.

(D) Bright-phase images of the infected cells. Scale bars, 100 μm.

(E) Volumes (mean ± SEM) of xenograft tumors from 1×10^5 infected cells. n = 6 independent experiments, $p < 0.01$, Student's t tests. Images of whole resected tumor xenograft tumors excised on day 25 (bottom). Scale bar, 10 mm.

(F) H&E staining and immunostaining of xenograft tumors, 25 days after transplantation. Scale bars, 100 μm.

**$p < 0.01$. See also Figure S2.

ALDH1A1 Expression Is Correlated with Poor Prognosis in Patients with Endometrial Cancer

To examine whether ALDH1A1 expression was associated with prognosis in clinical endometrial cancer, we determined the expression of ALDH1A1 in 258 clinical primary uterine endometrial endometrioid carcinoma tumor tissue samples by immunohistochemistry (Figure 5A). The clinicopathological characteristics are shown in Table S3. Immunostaining demonstrated that ALDH1A1 was expressed in more than 40% of tumor samples in patients with advanced-stage disease (stages III and IV), but was expressed only in 10% of patients with early-stage disease (stages I and II; Figure 5B). In addition, significantly higher levels of ALDH1A1 were observed in patients with high-grade endometrioid cancer than in patients with low-grade cancer (Figure 5B). Moreover, a fraction of ALDH1A1-expressed cells was higher in clinical specimens from advanced-stage or high-grade cancer than from early-stage or low-grade cancer (Figure 5C). Kaplan-Meier survival analyses of 35 patients with advanced-stage cancer showed that high ALDH1A1 expression was correlated with survival rate (Figure 5D, $p < 0.01$ for progression-free survival; Figure 5E, $p = 0.015$ for overall survival), consistent with previous reports (Huang et al., 2018; Rahadiani et al., 2011). Univariate and multivariate analyses revealed that positive ALDH1A1 staining was an independent prognostic factor of both progression-free and overall survival in patients with advanced-stage endometrial cancer

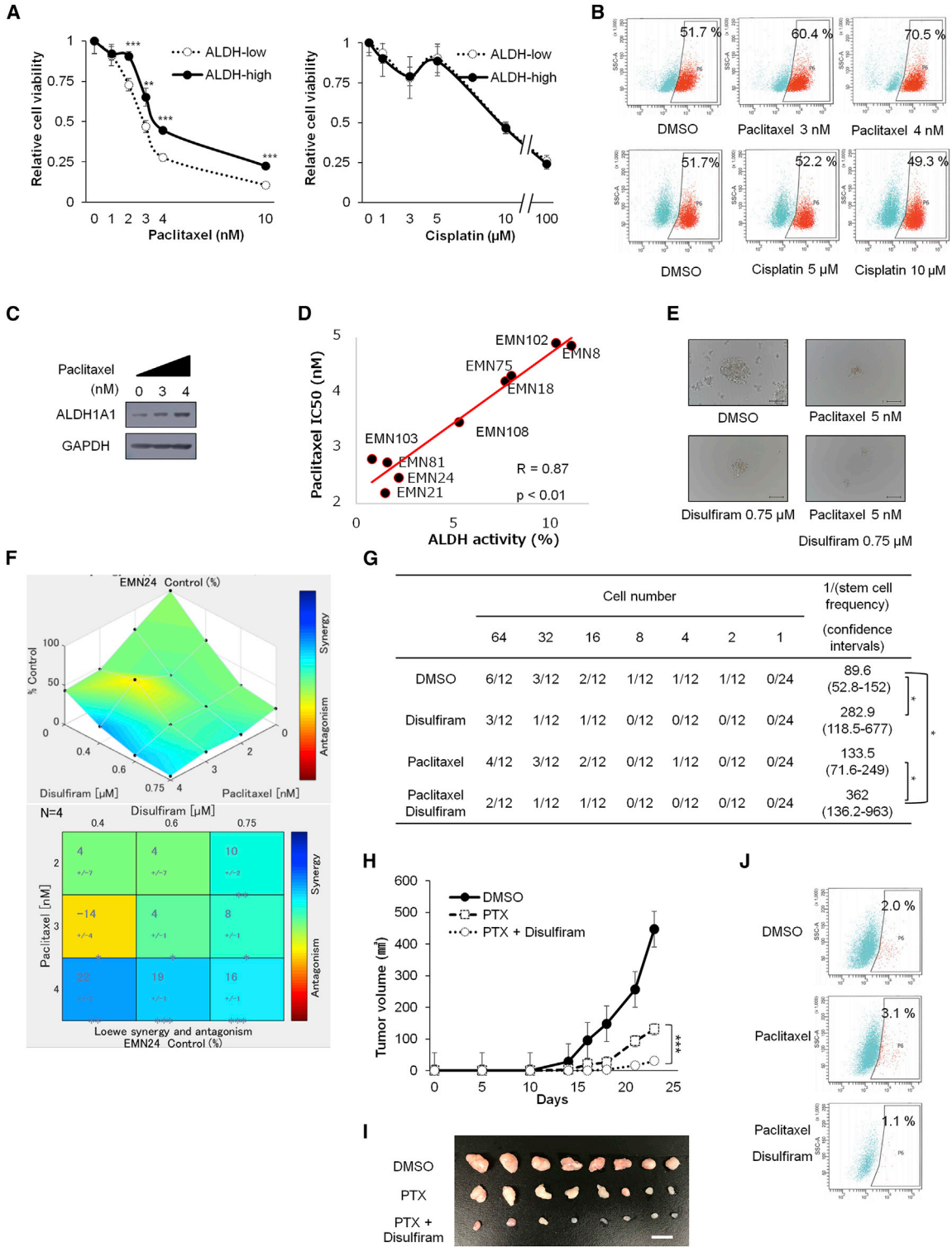

Figure 4. Combination Therapy with Paclitaxel and the ALDH Inhibitor Synergistically Inhibits Endometrial Cancer Cell Progression (EMN24 Cells)

(A) Responses of ALDH-high and ALDH-low cells to different concentrations of cisplatin and paclitaxel after treatment for 7 days. n = 4 independent experiments, Student's t test.

(legend continued on next page)

(Tables S4 and S5). These results indicated that ALDH1A1 expression was associated with pathological grade and poor prognosis.

Furthermore, we compared the expression levels of ALDH1A1 by immunostaining of paired uterine endometrial tumor samples before and after taxane-containing chemotherapy. Immunostaining analysis showed that, in six of ten patient samples, the ALDH1A1 staining area expanded more than five times after chemotherapy compared with that in matched tumor samples before chemotherapy (Figure 5F), thus further supporting the proposed role of ALDH-positive cells in paclitaxel resistance.

Spheroid Cells with ALDH Activity Show Glycolytic Dependency

Next, to gain an insight into mechanism by which ALDH function confers for the observed chemoresistance, we searched for biological pathways that were upregulated in cells with high levels of ALDH. GSEA showed the upregulation of glycolysis-related genes (hallmark of glycolysis) in the ALDH-high spheroid cells (Figure 6A). In fact, ALDH-high cells displayed higher levels of the extracellular acidification rate (ECAR) than ALDH-low cells (Figures 6B and S4A) and the treatment with disulfiram reduced ECAR (Figures 6C and S4B), indicating that glycolysis and glycolytic capacity were elevated in ALDH-high cells. In accordance with these results, glucose uptake, intracellular glucose, and lactate level were higher in ALDH-high cells than in ALDH-low cells (Figures 6D–6F and S4C–S4E) and suppressed by disulfiram (Figures 6D–6F and S4C–S4E). These data collectively indicate that spheroid cells with ALDH activity had increased glycolytic activity.

To examine whether reduced availability of glucose affects cell growth of ALDH-high cells, we cultivated ALDH-high and ALDH-low cells under glucose-free cultivation condition, and found that the reduced levels of glucose led to the relative suppression of cell growth in ALDH-high cells (Figure 6G) as well as the decrease of their proportion (Figure 6H). Similarly, 2-deoxy-D-glucose, an inhibitor of hexokinase, similarly suppressed cell growth of ALDH-high spheroid cells (Figure 6I). Thus, ALDH-high cells were more dependent on glycolytic function than ALDH-low cells for their survival and growth.

Glycolytic Suppression with GLUT1 Inhibition Suppressed Endometrial Cancer Stemness

Glucose transporters play an essential role in glucose influx, and 14 members of the glucose transporter (GLUT) family have been reported. Because some of the transporters are overexpressed or dysregulated in cancer cells (Zhao et al., 2013), we evaluated the differences in GLUT expression in ALDH-high and ALDH-low cells. Western blot analysis showed that GLUT1 was specifically expressed at higher levels in ALDH-high cells than in ALDH-low cells (Figures 7A and S4F). ALDH1A1 was responsible for GLUT1 expression because inhibition of ALDH1A1 decreased the expression of GLUT1 and exogenous ALDH1A1 overexpression led to the increase of GLUT1 expression (Figure 7A).

To examine whether GLUT1 mediates enhanced cell growth and stem-like property that is conferred by ALDH, we inhibited GLUT1 expression using shRNA lentiviral transfer (Figures 7B and S4G). After inhibition of GLUT1, repression of spheroid cell growth and glucose uptake were observed (Figures 7C–7E and S4H–S4J). In accordance, treatment with BAY876, a specific GLUT1 inhibitor, preferentially suppressed the cell viability and glucose uptake in ALDH-high cells (Figures 7F, 7G, S4K, and S4L). Inhibition of GLUT1 also decreased the expression of stemness markers, including Nanog, and c-myc (Figures 7B, 7H, S4G, and S4M). These data indicated that glucose uptake via GLUT1 is functionally important for the survival of ALDH-high endometrial CSCs.

Remarkably, inhibition of GLUT1 by RNAi or BAY876 sensitized spheroid cells to paclitaxel and synergistically suppressed the spheroid cell propagation *in vitro* (Figures 7I, 7J, S4N, and S4O) and tumor propagation *in vivo* (Figures 7K and 7L), thus phenocopying the effect of

(B) FACS analyses of ALDH activity in ALDH-high cells in the presence or absence of paclitaxel or cisplatin after *in vitro* treatment for 7 days.
(C) Western blot analyses of ALDH-high cells treated with paclitaxel for 7 days.
(D) Correlation between ALDH activity and paclitaxel half-maximal inhibitory concentration (nM).
(E) Bright-phase images of spheroids after *in vitro* paclitaxel and disulfiram treatment for 7 days. Scale bars, 100 μm.
(F) Relative cell viability of spheroid cells after culture for 7 days with the indicated concentrations of ALDH inhibitor and paclitaxel. Synergistic interaction was assessed with Combenefit software. n = 4 independent experiments.
(G) *In vitro* limiting dilution analysis over 14 days culture using spheroid cells exposed to 7 days treatment of disulfiram and/or paclitaxel *in vitro*.
(H) Volume (mean ± SEM) of xenograft tumors from 1×10^5 spheroid cells. Mice were separated into the vehicle (DMSO)-treated group, paclitaxel-treated group, and paclitaxel + disulfiram-treated group. n = 8 independent experiments, $p < 0.001$, Student's t test.
(I) Images of whole resected tumor xenografts excised on day 23. Scale bar, 10 mm.
(J) ALDH activity in cancer cells derived from xenograft tumors.
*$p < 0.05$; **$p < 0.01$; ***$p < 0.001$. See also Figure S3.

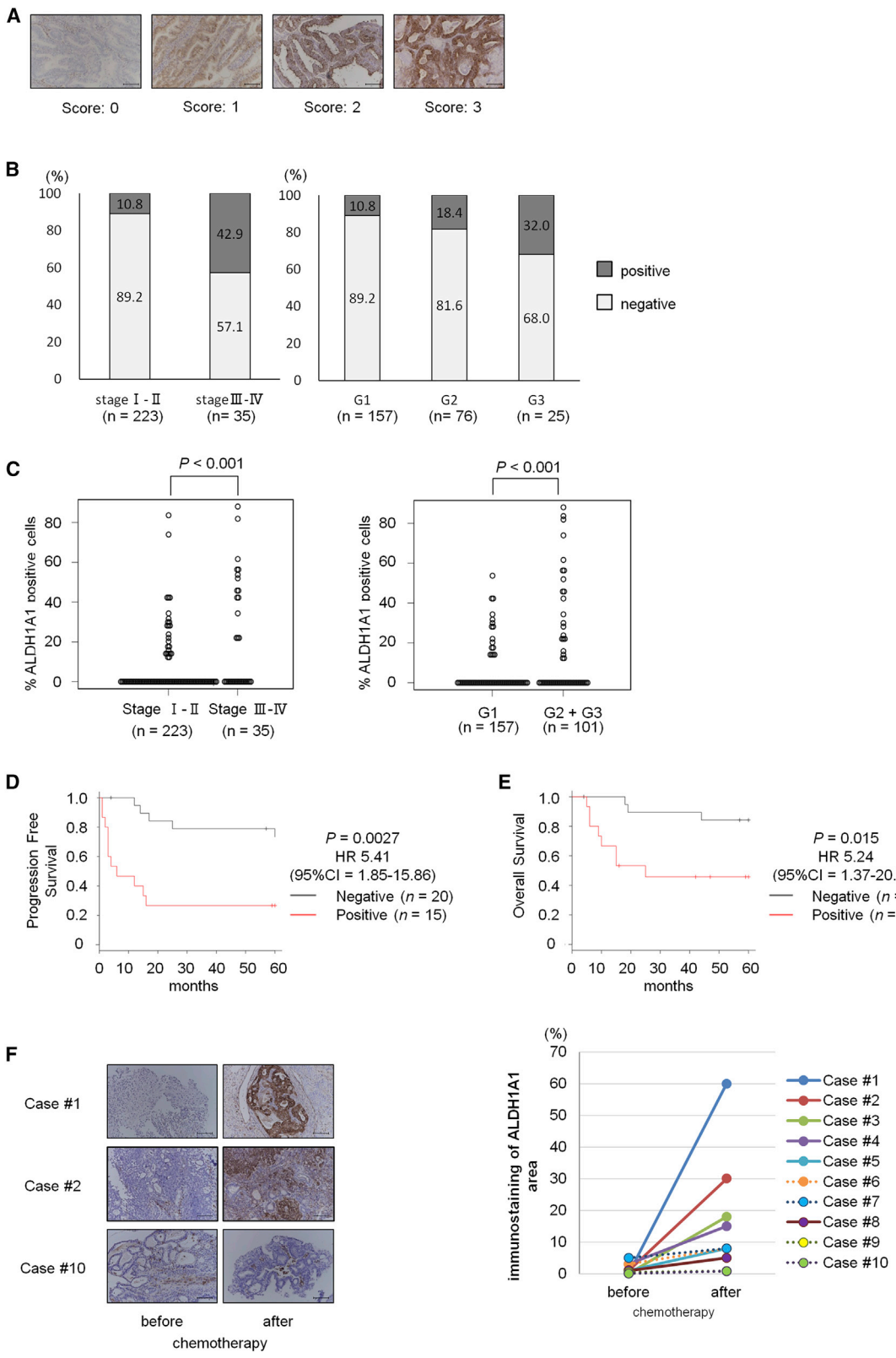

(legend on next page)

combination treatment of paclitaxel and disulfiram (Figures 4F, 4H, and S3E). These data indicate that GLUT1 mediates ALDH function to confer stem-like properties and paclitaxel resistance to the endometrial cancer spheroids.

Finally, to evaluate whether GLUT1 expression was associated with poor clinical outcome, we examined GLUT1 expression in clinical endometrial cancer tissue specimens by immunohistochemical staining (Figure 7M). We focused on advanced-stage cancer cases with high ALDH1A1 expression (n = 15), which were linked to poor prognosis (Figure 5). Kaplan-Meier survival analyses showed that high GLUT1 expression correlated with reduced survival rate (Figure 7N; p = 0.032 for progression-free survival; p = 0.04 for overall survival), suggesting that GLUT1 expression was associated with poor prognosis in advanced-stage endometrial cancer.

DISCUSSION

To develop novel clinical therapeutic strategies for refractory cancer, particularly for targeting CSCs, *in vitro* cultivation models can be invaluable tools. The floating spheroid culture method, which has been widely used for CSC research, retains characteristics of original tumors (Ishiguro et al., 2017). While short-term cultivation methods of three-dimensional cells from endometrial cancer tumor specimens (Girda et al., 2017; Kiyohara et al., 2016), and three-dimensional endometrial cancer cells after primary attachment cultivation in the presence of serum (Ding et al., 2017), have been reported previously, we demonstrated, for the first time, that endometrial cancer spheroids with CSC characteristics could be stably propagated *in vitro*. Notably, we observed that spheroid cells could be preferentially established from high-grade tumors. This is advantageous for clinical application because high-grade endometrial cancer with poor prognosis is associated with clinically relevant cells with malignant traits (Morice et al., 2016).

ALDH activity has been shown to be a specific marker of normal stem cells (Tomita et al., 2016) and various types of CSCs including endometrial cancer (Ginestier et al., 2007; Ishiguro et al., 2016; Kiyohara et al., 2017; Regan et al., 2017; van der Zee et al., 2015). It is not clear whether the functional importance can be expanded for other types of cancer, although the functional importance of ALDH activity has been shown for some cancer cells (Ishiguro et al., 2016; Liu et al., 2012a).

In this study, we demonstrated that ALDH-high endometrial cancer spheroid cells satisfied various criteria of CSCs. Functional analyses in endometrial spheroids showed that ALDH activity or ALDH1A1 expression promoted the proliferation and survival of endometrial CSCs. In addition, immunohistochemical studies of the clinical tumor showed that high levels of ALDH1A1 expression were associated with poor prognosis and advanced histological tumor grade in patients with endometrial cancer. These results suggested that ALDH1A1 expression facilitated the proliferation of endometrial CSCs, leading to a more aggressive and undifferentiated state in clinical tumors during disease progression (Lytle et al., 2018).

Resistance to current chemotherapy is one of the characteristics of CSCs, and chemotherapy preferentially selects CSC populations (Mueller et al., 2009; Lee et al., 2011; Hirst et al., 2018; Croker and Allan, 2012). Our data obtained from *in vitro* spheroids and clinical specimens showed that paclitaxel selectively increased the proportion of ALDH-high cells, indicating that ALDH-high endometrial CSCs were resistant to paclitaxel. These observations led us to examine the synergistic effects of paclitaxel and ALDH inhibitors, and we found that the combination therapy strongly suppressed the proliferation of endometrial cancer cells. Interestingly, increased levels of ALDH activity were observed in breast and ovarian cancer cells after paclitaxel exposure (Hirst et al., 2018; Park et al., 2015), and similar combination therapy was shown to be applicable in the treatment of taxane-resistant breast and ovarian cancer cells (Januchowski et al., 2016; Liu et al., 2013; Wu et al., 2019).

Figure 5. ALDH1 Expression Is Associated with Advanced Clinical Stage, Poor Prognosis, and Paclitaxel Sensitivity in Human Endometrial Cancer

(A) Representative immunostaining of ALDH1A1 (score 0–3). Scale bars, 100 μm.

(B) Distribution of ALDH1A1 expression during different clinical stages in endometrial cancer, and distribution of ALDH1A1 expression in different histological grades of endometrial cancer (n = 258).

(C) Percentage of ALDH1A1-expressed cancer cells in different clinical stage or histological grades of endometrial cancer (n = 258).

(D and E) Kaplan-Meier analyses of progression-free survival (D) and overall survival (E) in patients with advanced-stage endometrial cancer. The patients were stratified into ALDH1A1-positive (red lines, n = 15) and ALDH1A1-negative (gray lines, n = 20) groups. Most of these patients were treated with taxane-containing chemotherapy as the first-line regimen.

(F) Immunostaining for ALDH1A1 in uterine tumors before and after chemotherapy. Scale bars, 100 μm (left). ALDH1A1 immunostaining area in uterine tumors before and after chemotherapy (right). Cases of ALDH1A1 staining area expanded up to five times are indicated as straight lines (n = 6), and other cases are indicated as dotted lines (n = 4).

See also Table S3.

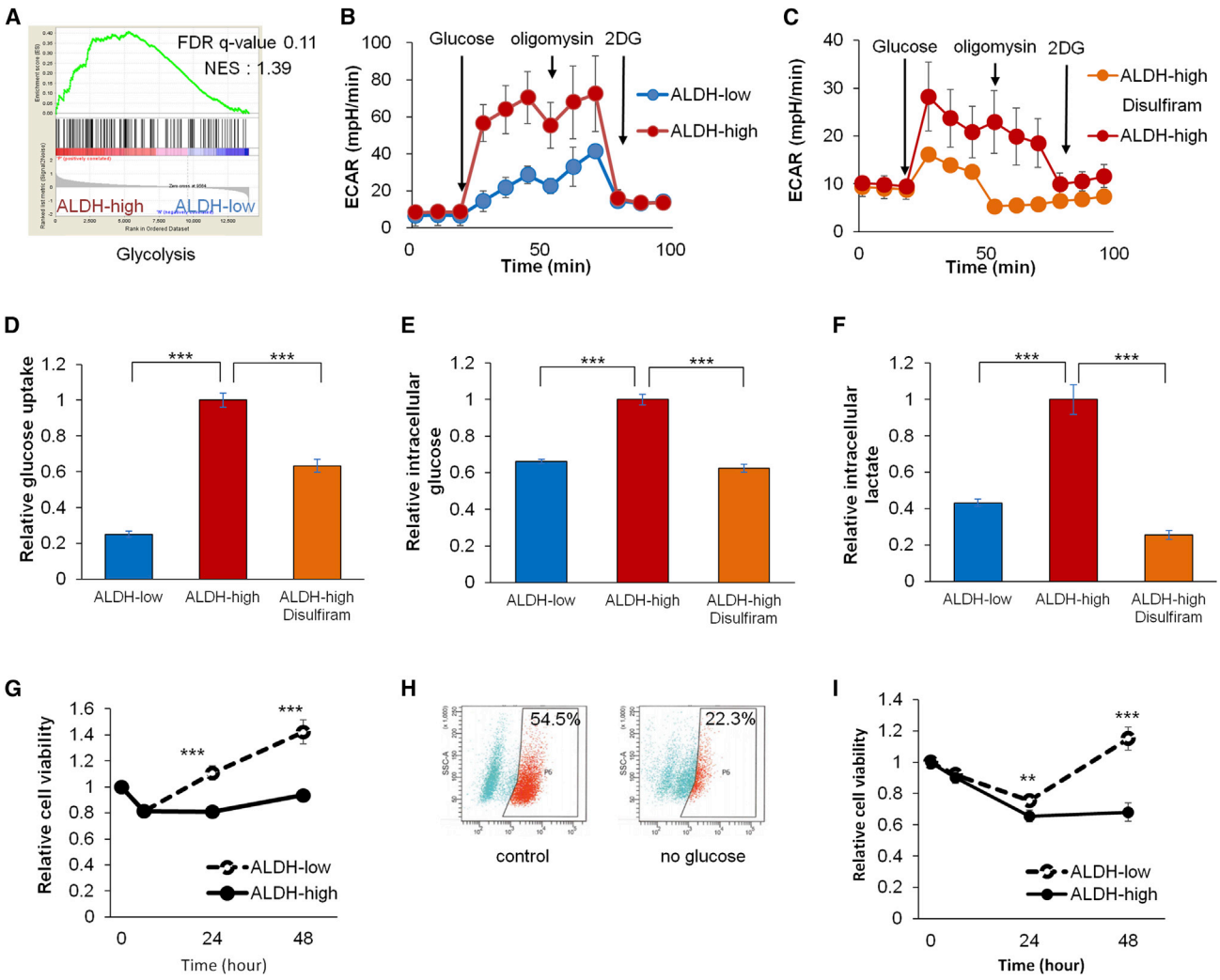

Figure 6. ALDH-High Endometrial Cancer Cells Depend on Glycolysis for Their Survival and Growth

(A) Gene set enrichment analyses of gene expression profiles between ALDH-high and ALDH-low cells (Hallmark of glycolysis).

(B and C) Time course of ECAR of spheroid cells with the indicated stimulation. The differences between ALDH-high and ALDH-low cells (B), and between ALDH-high cells with vehicle or disulfiram treatment (C). n = 4 independent experiments.

(D–F) Relative glucose uptake (D), intracellular glucose (E), and lactate level (F) of ALDH-low cells, ALDH-high cells, and ALDH-high cells treated with disulfiram. n = 4 independent experiments, $p < 0.01$, Student's t test.

(G) Time course of the proliferation of ALDH-high and ALDH-low cells under no glucose culture condition. n = 4 independent experiments, Student's t test.

(H) FACS analyses of ALDH activity in ALDH-high cells cultivated under normal or no glucose condition for 2 days.

(I) Time course of the proliferation of ALDH-high and ALDH-low cells under 20μM 2-deoxy-D-glucose (2-DG) treatment. n = 4 independent experiments, Student's t test.

**$p < 0.01$; ***$p < 0.001$. See also Figure S4.

It has been reported that, in many types of cancer, CSCs depend on enhanced glycolysis for their proliferation (Luo and Wicha, 2019; Liu et al., 2012b). Our data indicate that GLUT1 is a crucial downstream effector of ALDH, thus linking ALDH activation and glycolytic pathway in endometrial CSCs. It was previously shown that GLUT1 overexpression is commonly associated with cancer metabolism (Ancey et al., 2018). In addition, GLUT1 is essential for the self-renewal and tumor-initiating capacity of glioma CSCs (Shibuya et al., 2015), and GLUT inhibition and anti-cancer drug cooperated to suppress other types of cancer (Liu et al., 2012b). Hence, the ALDH-GLUT1 cascade may serve as a crucial pathway for the maintenance of CSCs and chemoresistance (Figure S4P). Because spheroids

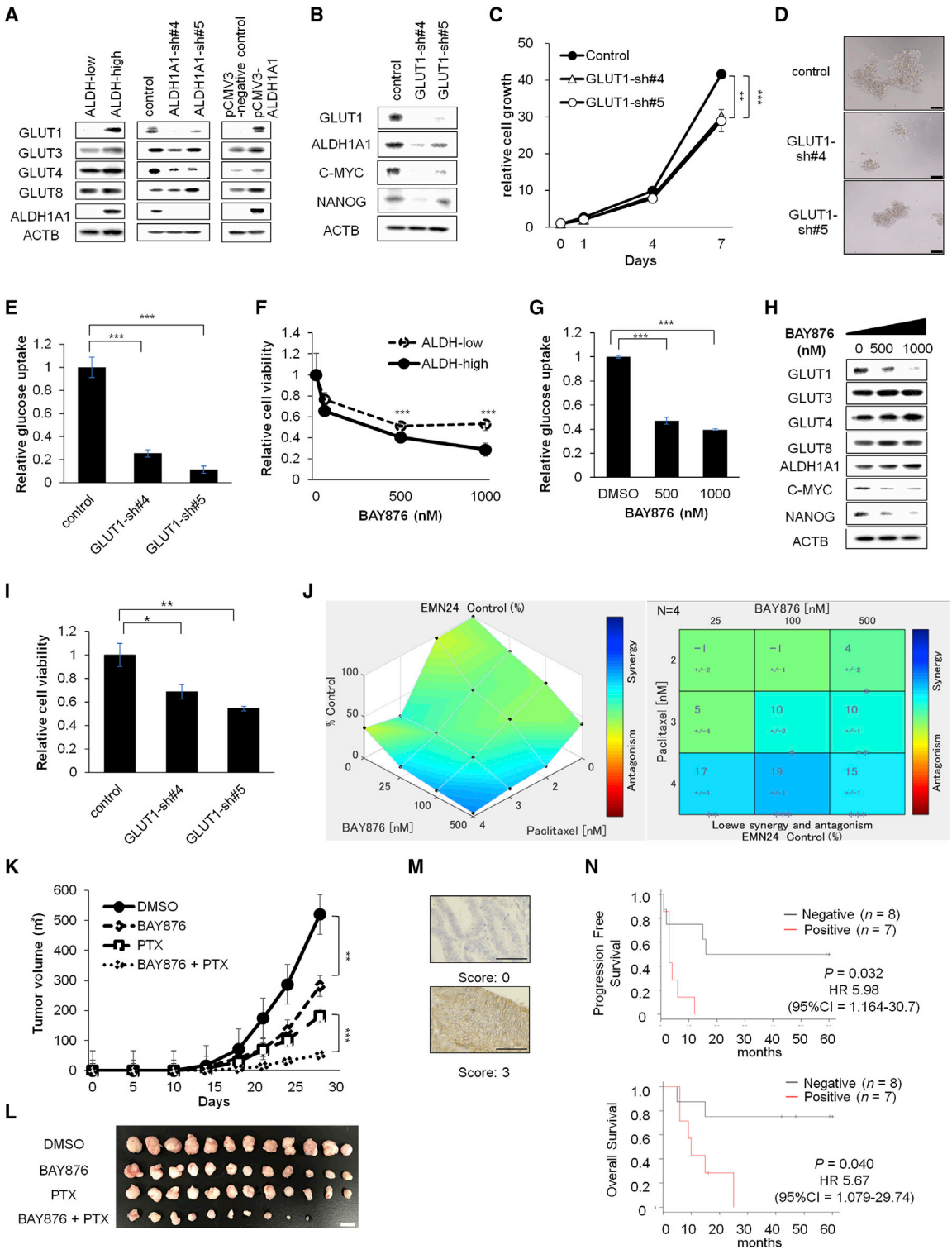

Figure 7. Combination Therapy with Paclitaxel and the GLUT1 Inhibitor Synergistically Inhibits Endometrial Cancer Cell Progression (EMN24 Cells)

(A and B) Western blot analyses of spheroid cells after indicated ALDH modification (A) and after GLUT1 inhibition (B).

(C) Time course of the proliferation of the infected cells. n = 4 independent experiments, $p < 0.01$, Student's t test.

(D) Bright-phase images of the infected cells. Scale bars, 100 μm.

(legend continued on next page)

presumably maintain characteristics similar to those of the original tumors, we expect that endometrial spheroids and spheroid-derived xenografts may have applications in personalized medicine in the future. To preclinically identify patients who may benefit from treatment with ALDH or GLUT inhibitors, our cultivation method may be useful for screening of clinical cases showing high levels of ALDH and hence respond to anti-ALDH or GLUT therapy in combination with taxane-derived compounds.

EXPERIMENTAL PROCEDURES

Tumor-Derived Spheroid Culture

All procedures were performed using protocols approved by the Ethics Committee of Niigata University and the National Cancer Center. Informed consent was obtained from all patients. Endometrial cancer cells from tumor samples were grown on ultra-low-attachment culture dishes (Corning, NY, USA) in StemPro hESC SFM (Gibco) supplemented with 8 ng/mL basic fibroblast growth factor (Invitrogen, Carlsbad, CA) and penicillin/streptomycin (37°C, 5% CO_2).

Animal Experiments

For cell transplantation assays in spheroid cells, the spheroids were dissociated into single cells with Accumax, suspended in 50 μL medium containing 50% Matrigel (BD Biosciences), and used for subcutaneous injection with a 27-G needle into the flanks of NOG (NOD/Shi-scid IL-2Rγnull) mice (Central Institute for Experimental Animals, Kawasaki, Japan). All mouse procedures were approved by the Animal Care and Use Committees of Niigata University and performed in accordance with institutional policies.

Lentivirus-Mediated Short Hairpin RNA Transduction

Lentivirus plasmid expressing ALDH1A1 short hairpin RNAs (shRNAs) (sh4, TRCN0000276460; sh5, TRCN0000276461), GLUT1 shRNAs (sh4, TRCN0000424030; sh5, TRCN0000423590), and control shRNA were purchased from Sigma. The pCMV3-ALDH1A1 plasmid (HG11388-UT) and pCMV3 control vector were purchased from Sino Biological. Preparation of virus-containing supernatants and virus infection were performed as previously described (Ishiguro et al., 2016). Cells infected with the viruses were selected in the presence of 2 μg/mL puromycin or 100 μg/mL hygromycin.

Western Blot Analyses

Cells were lysed in RIPA buffer (50 mM Tris [pH 8.0], 150 mM NaCl, 1% Nonidet P-40, 0.5% sodium deoxycholate, 0.1% SDS, and 1 mM EDTA) supplemented with protease inhibitors (Roche) and used for Western blot analysis, as described previously (Ishiguro et al., 2016), with primary antibodies (Table S6).

Statistical Analyses

For statistical analyses of spheroid cell experiments, Welch t tests or Student's t tests were performed based on the results of F tests. Differences with p values of less than 0.05 were considered significant. *$p < 0.05$, **$p < 0.01$, ***$p < 0.001$. Statistical analyses of clinical samples were performed using EZR (Kanda, 2013). Univariate survival analysis was performed using the Kaplan-Meier method, and the significance of difference between groups was examined using log rank tests. Multivariate survival analysis was carried out using the Cox proportional hazards regression model. Hazard ratios and 95% confidence intervals were calculated with Cox's proportional hazards regression model. Variables with p values of less than 0.05 on univariate regression analysis were examined in multivariate regression analysis.

Additional materials and methods can be retrieved in Supplemental Experimental Procedures.

SUPPLEMENTAL INFORMATION

Supplemental Information can be found online at https://doi.org/10.1016/j.stemcr.2019.08.015.

AUTHOR CONTRIBUTIONS

Conception and design, Y.M., K.Yamawaki, T.I., and T.E. Development of methodology, Y.M., K.Yamawaki, T.I., A.S., and H.O. Acquisition of data, Y.M., K.Yamawaki, T.I., and H.U. Analysis

(E) Glucose uptake of spheroid cells of the infected cells. n = 4 independent experiments, $p < 0.01$, Student's t test.
(F and G) Relative cell viability (F) and glucose uptake (G) of spheroid cells after culture for 7 days with the indicated concentration of BAY876. n = 4 independent experiments, $p < 0.01$, Student's t test.
(H) Western blot analyses of spheroid cells after exposure to the indicated concentration of BAY876.
(I) Relative cell viability of spheroid cells after culture for 7 days with 2 nM paclitaxel. n = 4 independent experiments, $p < 0.01$, Student's t test.
(J) Relative cell viability of spheroid cells with the indicated concentrations of BAY876 and paclitaxel *in vitro*. Synergistic interaction was assessed with Combenefit software. n = 4 independent experiments.
(K) Volume (mean ± SEM) of xenograft tumors from 1×10^5 spheroid cells. Mice were separated into the vehicle (DMSO)-treated group, paclitaxel-treated group, BAY876-treated group, and paclitaxel + BAY876-treated group. n = 12 independent experiments, $p < 0.001$, Student's t test.
(L) Images of whole resected tumor xenografts excised on day 23. Scale bar, 10 mm.
(M) Representative immunostaining of GLUT1. Scale bars, 100 μm.
(N) Kaplan-Meier analyses of progression-free survival (upper) and overall survival (lower) in patients with advanced-stage ALDH-positive endometrial cancer. The patients were stratified into GLUT1-high (red lines, n = 7) and GLUT1-low (gray lines, n = 8) groups.
*$p < 0.05$; **$p < 0.01$; ***$p < 0.001$. See also Figure S4.

and interpretation of data, Y.M., K.Yamawaki, T.I., K.Yoshihara, Y.Y., and T.M. Writing, review, and/or revision of the manuscript, Y.M., K.Yamawaki, T.I., K.Yoshihara, H.U., A.S., H.O., K.O., and T.E. Study supervision, K.O. and T.E.

ACKNOWLEDGMENTS

We thank Ryo Tamura, Kazuaki Suda, Kentaro Sugino, Manako Yamaguchi, Nozomi Yachida, Anna Ishida, Nobumichi Nishikawa, and Masayuki Sekine (Department of Obstetrics and Gynecology, Niigata University Graduate School of Medical and Dental Sciences), Ippei Shimizu (Department of Cardiovascular Biology and Medicine, Niigata University Graduate School of Medical and Dental Sciences), and Hiroaki Sakai (National Cancer Center Research Institute) for scientific advice and technical assistance. They disclose no potential conflicts of interest. This research was supported by Grants-in-Aid for Young Scientists (B) (grant no. 15K20132) and Scientific Research (C) (grant no. 18K09250) to T.I. from the Japan Society for the Promotion of Science and the Tsukada Grant for Niigata University Medical Research to T.I. This work was partially supported by the National Cancer Center Research and Development Funds (29-A-2).

Received: January 14, 2019
Revised: August 28, 2019
Accepted: August 29, 2019
Published: September 26, 2019

REFERENCES

Ancey, P.B., Contat, C., and Meylan, E. (2018). Glucose transporters in cancer—from tumor cells to the tumor microenvironment. FEBS J. *285*, 2926–2943.

Aoki, D. (2014). Annual report of Gynecologic Oncology Committee, Japan Society of Obstetrics and Gynecology, 2013. J. Obstet. Gynaecol. Res. *40*, 338–348.

Ben-Porath, I., Thomson, M.W., Carey, V.J., Ge, R., Bell, G.W., Regev, A., and Weinberg, R.A. (2008). An embryonic stem cell-like gene expression signature in poorly differentiated aggressive human tumors. Nat. Genet. *40*, 499–507.

Bestvina, C.M., and Fleming, G.F. (2016). Chemotherapy for endometrial cancer in adjuvant and advanced disease settings. Oncologist *21*, 1250–1259.

Croker, A.K., and Allan, A.L. (2012). Inhibition of aldehyde dehydrogenase (ALDH) activity reduces chemotherapy and radiation resistance of stem-like ALDHhiCD44(+) human breast cancer cells. Breast Cancer Res. Treat. *133*, 75–87.

de Boer, S.M., Powell, M.E., Mileshkin, L., Katsaros, D., Bessette, P., Haie-Meder, C., Ottevanger, P.B., Ledermann, J.A., Khaw, P., Colombo, A., et al. (2018). Adjuvant chemoradiotherapy versus radiotherapy alone for women with high-risk endometrial cancer (PORTEC-3): final results of an international, open-label, multicentre, randomised, phase 3 trial. Lancet Oncol. *19*, 295–309.

Ding, D.C., Liu, H.W., Chang, Y.H., and Chu, T.Y. (2017). Expression of CD133 in endometrial cancer cells and its implications. J. Cancer *8*, 2142–2153.

Dontu, G., Abdallah, W.M., Foley, J.M., Jackson, K.W., Clarke, M.F., Kawamura, M.J., and Wicha, M.S. (2003). In vitro propagation and transcriptional profiling of human mammary stem/progenitor cells. Genes Dev. *17*, 1253–1270.

Ginestier, C., Hur, M.H., Charafe-Jauffret, E., Monville, F., Dutcher, J., Brown, M., Jacquemier, J., Viens, P., Kleer, C.G., Liu, S., et al. (2007). ALDH1 is a marker of normal and malignant human mammary stem cells and a predictor of poor clinical outcome. Cell Stem Cell *1*, 555–567.

Girda, E., Huang, E.C., Leiserowitz, G.S., and Smith, L.H. (2017). The use of endometrial cancer patient-derived organoid culture for drug sensitivity testing is feasible. Int. J. Gynecol. Cancer *27*, 1701–1707.

Hida, K., Maishi, N., Akiyama, K., Ohmura-Kakutani, H., Torii, C., Ohga, N., Osawa, T., Kikuchi, H., Morimoto, H., Morimoto, M., et al. (2017). Tumor endothelial cells with high aldehyde dehydrogenase activity show drug resistance. Cancer Sci. *108*, 2195–2203.

Hirst, J., Pathak, H.B., Hyter, S., Pessetto, Z.Y., Ly, T., Graw, S., Koestler, D.C., Krieg, A.J., Roby, K.F., and Godwin, A.K. (2018). Licofelone enhances the efficacy of paclitaxel in ovarian cancer by reversing drug resistance and tumor stem-like properties. Cancer Res. *78*, 4370–4385.

House, C.D., Jordan, E., Hernandez, L., Ozaki, M., James, J.M., Kim, M., Kruhlak, M.J., Batchelor, E., Elloumi, F., Cam, M.C., et al. (2017). NFkappaB promotes ovarian tumorigenesis via classical pathways that support proliferative cancer cells and alternative pathways that support ALDH(+) cancer stem-like cells. Cancer Res. *77*, 6927–6940.

Huang, H.H., Wang, Y.C., Chou, Y.C., Yu, M.H., and Chao, T.K. (2018). The combination of aldehyde dehydrogenase 1 (ALDH1) and CD44 is associated with poor outcomes in endometrial cancer. PLoS One *13*, e0206685.

Hubbard, S.A., Friel, A.M., Kumar, B., Zhang, L., Rueda, B.R., and Gargett, C.E. (2009). Evidence for cancer stem cells in human endometrial carcinoma. Cancer Res. *69*, 8241–8248.

Ishiguro, T., Sato, A., Ohata, H., Ikarashi, Y., Takahashi, R.U., Ochiya, T., Yoshida, M., Tsuda, H., Onda, T., Kato, T., et al. (2016). Establishment and characterization of an in vitro model of ovarian cancer stem-like cells with an enhanced proliferative capacity. Cancer Res. *76*, 150–160.

Ishiguro, T., Ohata, H., Sato, A., Yamawaki, K., Enomoto, T., and Okamoto, K. (2017). Tumor-derived spheroids: relevance to cancer stem cells and clinical applications. Cancer Sci. *108*, 283–289.

Januchowski, R., Wojtowicz, K., Sterzyska, K., Sosiska, P., Andrzejewska, M., Zawierucha, P., Nowicki, M., and Zabel, M. (2016). Inhibition of ALDH1A1 activity decreases expression of drug transporters and reduces chemotherapy resistance in ovarian cancer cell lines. Int. J. Biochem. Cell Biol. *78*, 248–259.

Kanda, Y. (2013). Investigation of the freely available easy-to-use software 'EZR' for medical statistics. Bone Marrow Transplant *48*, 452–458.

Kiyohara, Y., Yoshino, K., Kubota, S., Okuyama, H., Endo, H., Ueda, Y., Kimura, T., Kimura, T., Kamiura, S., and Inoue, M. (2016). Drug screening and grouping by sensitivity with a panel of primary

cultured cancer spheroids derived from endometrial cancer. Cancer Sci. *107*, 452–460.

Kiyohara, M.H., Dillard, C., Tsui, J., Kim, S.R., Lu, J., Sachdev, D., Goodglick, L., Tong, M., Torous, V.F., Aryasomayajula, C., et al. (2017). EMP2 is a novel therapeutic target for endometrial cancer stem cells. Oncogene *36*, 5793–5807.

Lee, T.K., Castilho, A., Cheung, V.C., Tang, K.H., Ma, S., and Ng, I.O. (2011). CD24(+) liver tumor-initiating cells drive self-renewal and tumor initiation through STAT3-mediated NANOG regulation. Cell Stem Cell *9*, 50–63.

Liu, P., Brown, S., Goktug, T., Channathodiyil, P., Kannappan, V., Hugnot, J.P., Guichet, P.O., Bian, X., Armesilla, A.L., Darling, J.L., et al. (2012a). Cytotoxic effect of disulfiram/copper on human glioblastoma cell lines and ALDH-positive cancer-stem-like cells. Br. J. Cancer *107*, 1488–1497.

Liu, Y., Cao, Y., Zhang, W., Bergmeier, S., Qian, Y., Akbar, H., Colvin, R., Ding, J., Tong, L., Wu, S., et al. (2012b). A small-molecule inhibitor of glucose transporter 1 downregulates glycolysis, induces cell-cycle arrest, and inhibits cancer cell growth in vitro and in vivo. Mol. Cancer Ther. *11*, 1672–1682.

Liu, P., Kumar, I.S., Brown, S., Kannappan, V., Tawari, P.E., Tang, J.Z., Jiang, W., Armesilla, A.L., Darling, J.L., and Wang, W. (2013). Disulfiram targets cancer stem-like cells and reverses resistance and cross-resistance in acquired paclitaxel-resistant triple-negative breast cancer cells. Br. J. Cancer *109*, 1876–1885.

Lonardo, E., Hermann, P.C., Mueller, M.T., Huber, S., Balic, A., Miranda-Lorenzo, I., Zagorac, S., Alcala, S., Rodriguez-Arabaolaza, I., Ramirez, J.C., et al. (2011). Nodal/Activin signaling drives self-renewal and tumorigenicity of pancreatic cancer stem cells and provides a target for combined drug therapy. Cell Stem Cell. *9*, 433–446.

Luo, M., and Wicha, M.S. (2019). Targeting cancer stem cell redox metabolism to enhance therapy responses. Semin. Radiat. Oncol. *29*, 42–54.

Lytle, N.K., Barber, A.G., and Reya, T. (2018). Stem cell fate in cancer growth, progression and therapy resistance. Nat. Rev. Cancer *18*, 669–680.

Morice, P., Leary, A., Creutzberg, C., Abu-Rustum, N., and Darai, E. (2016). Endometrial cancer. Lancet *387*, 1094–1108.

Mueller, M.T., Hermann, P.C., Witthauer, J., Rubio-Viqueira, B., Leicht, S.F., Huber, S., Ellwart, J.W., Mustafa, M., Bartenstein, P., D'Haese, J.G., et al. (2009). Combined targeted treatment to eliminate tumorigenic cancer stem cells in human pancreatic cancer. Gastroenterology *137*, 1102–1113.

Nechushtan, H., Hamamreh, Y., Nidal, S., Gotfried, M., Baron, A., Shalev, Y.I., Nisman, B., Peretz, T., and Peylan-Ramu, N. (2015). A phase IIb trial assessing the addition of disulfiram to chemotherapy for the treatment of metastatic non-small cell lung cancer. Oncologist *20*, 366–367.

Nomura, H., Aoki, D., Takahashi, F., Katsumata, N., Watanabe, Y., Konishi, I., Jobo, T., Hatae, M., Hiura, M., and Yaegashi, N. (2011). Randomized phase II study comparing docetaxel plus cisplatin, docetaxel plus carboplatin, and paclitaxel plus carboplatin in patients with advanced or recurrent endometrial carcinoma: a Japanese Gynecologic Oncology Group study (JGOG2041). Ann. Oncol. *22*, 636–642.

Ohata, H., Ishiguro, T., Aihara, Y., Sato, A., Sakai, H., Sekine, S., Taniguchi, H., Akasu, T., Fujita, S., Nakagama, H., et al. (2012). Induction of the stem-like cell regulator CD44 by Rho kinase inhibition contributes to the maintenance of colon cancer-initiating cells. Cancer Res. *72*, 5101–5110.

Park, S.Y., Kim, M.J., Park, S.A., Kim, J.S., Min, K.N., Kim, D.K., Lim, W., Nam, J.S., and Sheen, Y.Y. (2015). Combinatorial TGF-beta attenuation with paclitaxel inhibits the epithelial-to-mesenchymal transition and breast cancer stem-like cells. Oncotarget *6*, 37526–37543.

Pastrana, E., Silva-Vargas, V., and Doetsch, F. (2011). Eyes wide open: a critical review of sphere-formation as an assay for stem cells. Cell Stem Cell *8*, 486–498.

Pece, S., Tosoni, D., Confalonieri, S., Mazzarol, G., Vecchi, M., Ronzoni, S., Bernard, L., Viale, G., Pelicci, P.G., and Di Fiore, P.P. (2010). Biological and molecular heterogeneity of breast cancers correlates with their cancer stem cell content. Cell *140*, 62–73.

Rahadiani, N., Ikeda, J., Mamat, S., Matsuzaki, S., Ueda, Y., Umehara, R., Tian, T., Wang, Y., Enomoto, T., Kimura, T., et al. (2011). Expression of aldehyde dehydrogenase 1 (ALDH1) in endometrioid adenocarcinoma and its clinical implications. Cancer Sci. *102*, 903–908.

Regan, J.L., Schumacher, D., Staudte, S., Steffen, A., Haybaeck, J., Keilholz, U., Schweiger, C., Golob-Schwarzl, N., Mumberg, D., Henderson, D., et al. (2017). Non-canonical Hedgehog signaling is a positive regulator of the WNT pathway and is required for the survival of colon cancer stem cells. Cell Rep. *21*, 2813–2828.

Ricci-Vitiani, L., Lombardi, D.G., Pilozzi, E., Biffoni, M., Todaro, M., Peschle, C., and De Maria, R. (2007). Identification and expansion of human colon-cancer-initiating cells. Nature *445*, 111–115.

Rutella, S., Bonanno, G., Procoli, A., Mariotti, A., Corallo, M., Prisco, M.G., Eramo, A., Napoletano, C., Gallo, D., Perillo, A., et al. (2009). Cells with characteristics of cancer stem/progenitor cells express the CD133 antigen in human endometrial tumors. Clin. Cancer Res. *15*, 4299–4311.

Safi, R., Nelson, E.R., Chitneni, S.K., Franz, K.J., George, D.J., Zalutsky, M.R., and McDonnell, D.P. (2014). Copper signaling axis as a target for prostate cancer therapeutics. Cancer Res. *74*, 5819–5831.

Shibuya, K., Okada, M., Suzuki, S., Seino, M., Seino, S., Takeda, H., and Kitanaka, C. (2015). Targeting the facilitative glucose transporter GLUT1 inhibits the self-renewal and tumor-initiating capacity of cancer stem cells. Oncotarget *6*, 651–661.

Siegel, R.L., Miller, K.D., and Jemal, A. (2015). Cancer statistics, 2015. CA Cancer J. Clin. *65*, 5–29.

Singh, S.K., Clarke, I.D., Terasaki, M., Bonn, V.E., Hawkins, C., Squire, J., and Dirks, P.B. (2003). Identification of a cancer stem cell in human brain tumors. Cancer Res. *63*, 5821–5828.

Soumerai, T.E., Donoghue, M.T.A., Bandlamudi, C., Srinivasan, P., Chang, M.T., Zamarin, D., Cadoo, K.A., Grisham, R.N., O'Cearbhaill, R.E., Tew, W.P., et al. (2018). Clinical utility of prospective molecular characterization in advanced endometrial cancer. Clin. Cancer Res. *24*, 5939–5947.

The Cancer Genome Atlas Network (2013). Integrated genomic characterization of endometrial carcinoma. Nature *497*, 67–73.

Tomita, H., Tanaka, K., Tanaka, T., and Hara, A. (2016). Aldehyde dehydrogenase 1A1 in stem cells and cancer. Oncotarget *7*, 11018–11032.

Valent, P., Bonnet, D., De Maria, R., Lapidot, T., Copland, M., Melo, J.V., Chomienne, C., Ishikawa, F., Schuringa, J.J., Stassi, G., et al. (2012). Cancer stem cell definitions and terminology: the devil is in the details. Nat. Rev. Cancer *12*, 767–775.

van der Zee, M., Sacchetti, A., Cansoy, M., Joosten, R., Teeuwssen, M., Heijmans-Antonissen, C., Ewing-Graham, P.C., Burger, C.W., Blok, L.J., and Fodde, R. (2015). IL6/JAK1/STAT3 signaling blockade in endometrial cancer affects the ALDHhi/CD126+ stem-like component and reduces tumor burden. Cancer Res. *75*, 3608–3622.

Wong, D.J., Liu, H., Ridky, T.W., Cassarino, D., Segal, E., and Chang, H.Y. (2008). Module map of stem cell genes guides creation of epithelial cancer stem cells. Cell Stem Cell *2*, 333–344.

Wu, L., Meng, F., Dong, L., Block, C.J., Mitchell, A.V., Wu, J., Jang, H., Chen, W., Polin, L., Yang, Q., et al. (2019). Disulfiram and BKM120 in combination with chemotherapy impede tumor progression and delay tumor recurrence in tumor initiating cell-rich TNBC. Sci. Rep. *9*, 236.

Xu, B., Wang, S., Li, R., Chen, K., He, L., Deng, M., Kannappan, V., Zha, J., Dong, H., and Wang, W. (2017). Disulfiram/copper selectively eradicates AML leukemia stem cells in vitro and in vivo by simultaneous induction of ROS-JNK and inhibition of NF-kappaB and Nrf2. Cell Death Dis. *8*, e2797.

Yip, N.C., Fombon, I.S., Liu, P., Brown, S., Kannappan, V., Armesilla, A.L., Xu, B., Cassidy, J., Darling, J.L., and Wang, W. (2011). Disulfiram modulated ROS-MAPK and NFkappaB pathways and targeted breast cancer cells with cancer stem cell-like properties. Br. J. Cancer *104*, 1564–1574.

Zhao, Y., Butler, E.B., and Tan, M. (2013). Targeting cellular metabolism to improve cancer therapeutics. Cell Death Dis. *4*, e532.

Stem Cell Reports, Volume *13*

Supplemental Information

ALDH-Dependent Glycolytic Activation Mediates Stemness and Paclitaxel Resistance in Patient-Derived Spheroid Models of Uterine Endometrial Cancer

Yutaro Mori, Kaoru Yamawaki, Tatsuya Ishiguro, Kosuke Yoshihara, Haruka Ueda, Ai Sato, Hirokazu Ohata, Yohko Yoshida, Tohru Minamino, Koji Okamoto, and Takayuki Enomoto

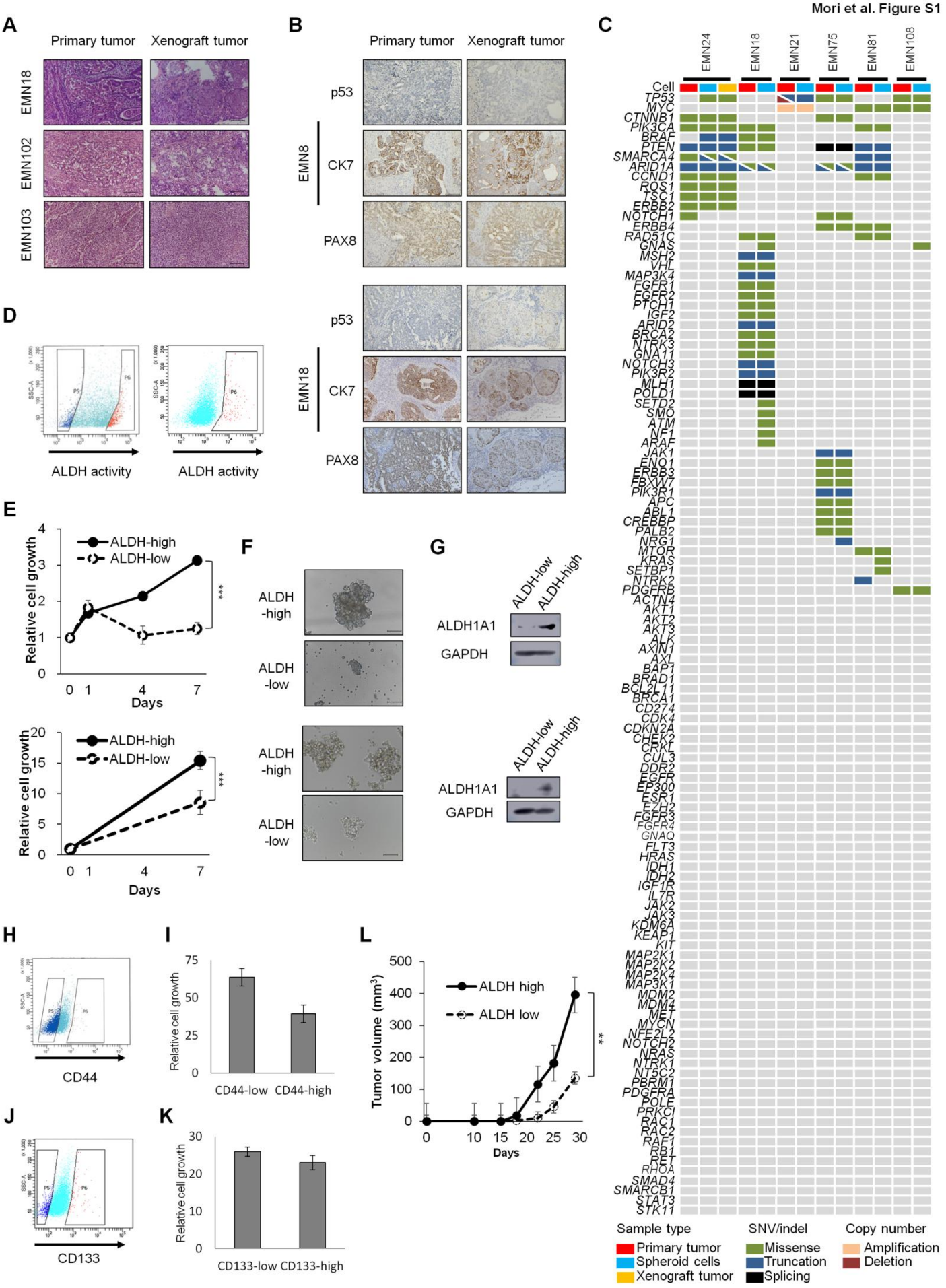
A
Primary tumor
Xenograft tumor
EMN18
EMN102
EMN103
B
Primary tumor
Xenograft tumor
p53
EMN8
CK7
PAX8
p53
EMN18
CK7
PAX8
C
EMN24
EMN18
EMN21
EMN75
EMN81
EMN108
Cell
TP53
MYC
CTNNB1
PIK3CA
BRAF
PTEN
SMARCA4
ARID1A
CCND1
ROS1
TSC1
ERBB2
NOTCH1
ERBB4
RAD51C
GNAS
MSH2
VHL
MAP3K4
FGFR1
FGFR2
PTCH1
IGF2
ARID2
BRCA2
NTRK3
GNA11
NOTCH3
PIK3R2
MLH1
POLD1
SETD2
SMO
ATM
NF1
ARAF
JAK1
ENO1
ERBB3
FBXW7
PIK3R1
APC
ABL1
CREBBP
PALB2
NRG1
MTOR
KRAS
SETBP1
NTRK2
PDGFRB
ACTN4
AKT1
AKT2
AKT3
ALK
AXIN1
AXL
BAP1
BRAD1
BCL2L11
BRCA1
CD274
CDK4
CDKN2A
CHEK2
CRKL
CUL3
DDR2
EGFR
EP300
ESR1
EZH2
FGFR3
FGFR4
GNAQ
FLT3
HRAS
IDH1
IDH2
IGF1R
IL7R
JAK2
JAK3
KDM6A
KEAP1
KIT
MAP2K1
MAP2K2
MAP2K4
MAP3K1
MDM2
MDM4
MET
MYCN
NFE2L2
NOTCH2
NRAS
NTRK1
NT5C2
PBRM1
PDGFRA
POLE
PRKCI
RAC1
RAC2
RAF1
RB1
RET
RHOA
SMAD4
SMARCB1
STAT3
STK11
Sample type
Primary tumor
Spheroid cells
Xenograft tumor
SNV/indel
Missense
Truncation
Splicing
Copy number
Amplification
Deletion
D
ALDH activity
ALDH activity
E
ALDH-high
ALDH-low
Relative cell growth
Days
***
ALDH-high
ALDH-low
Relative cell growth
Days
***
F
ALDH -high
ALDH -low
ALDH -high
ALDH -low
G
ALDH-low
ALDH-high
ALDH1A1
GAPDH
ALDH-low
ALDH-high
ALDH1A1
GAPDH
H
CD44
I
Relative cell growth
CD44-low
CD44-high
J
CD133
K
Relative cell growth
CD133-low
CD133-high
L
ALDH high
ALDH low
Tumor volume (mm3)
Days
**

Figure S1. Spheroid cells derived from human endometrial cancer showing the characteristics of CSCs with high ALDH activity. Related to Figure 1.

A, H&E staining of xenograft and primary tumors (EMN18, EMN102, and EMN103 cells). Scale bar, 100 μm. B, Immunostaining of xenograft and primary tumors with the indicated antibodies (EMN8 and EMN18 cells). Scale bar, 100 μm. C, Target sequencing analyses of primary tumor and spheroid cells. D, FACS analyses of ALDH activity after ALDEFLUOR staining (Left: EMN 8, Right: EMN21). Left gated population, ALDH-low cells; right gated population, ALDH-high cells (EMN8 cells). E, time course analyses of cell growth (Upper: EMN8, Lower: EMN21). n = 4 independent experiments, $p < 0.001$, Student's t-tests. F, Bright-phase images of spheroid formation after 7 days of *in vitro* cultivation (Upper: EMN8, Lower: EMN21). Scale bars, 100 μm. G, Western blot analyses of ALDH-high and ALDH-low cells after sorting (Upper: EMN8, Lower: EMN21). H, FACS analyses of CD44 expression (EMN24 cells). Left gated population, CD44-low cells; right gated population, CD44-high cells. I, Relative number of spheroid cells after *in vitro* cultivation for 7 days after sorting based on CD44 expression (EMN24 cells). n = 4 independent experiments, Student's t-tests. J, FACS analyses of CD133 expression (EMN24 cells). Left gated population, CD133-low cells; right gated population, CD133-high cells. K, Relative number of spheroid cells after *in vitro* cultivation for 7 days after sorting based on CD133 expression (EMN24 cells). n = 4 independent experiments, Student's t-tests. L, Volume (mean ± SEM) of xenograft tumors from 1×10^6 ALDH-low and ALDH-high cells (EMN21). n = 5 independent experiments, $p = 0.002$, Student's t-tests. **, $p < 0.01$; ***, $p < 0.001$.

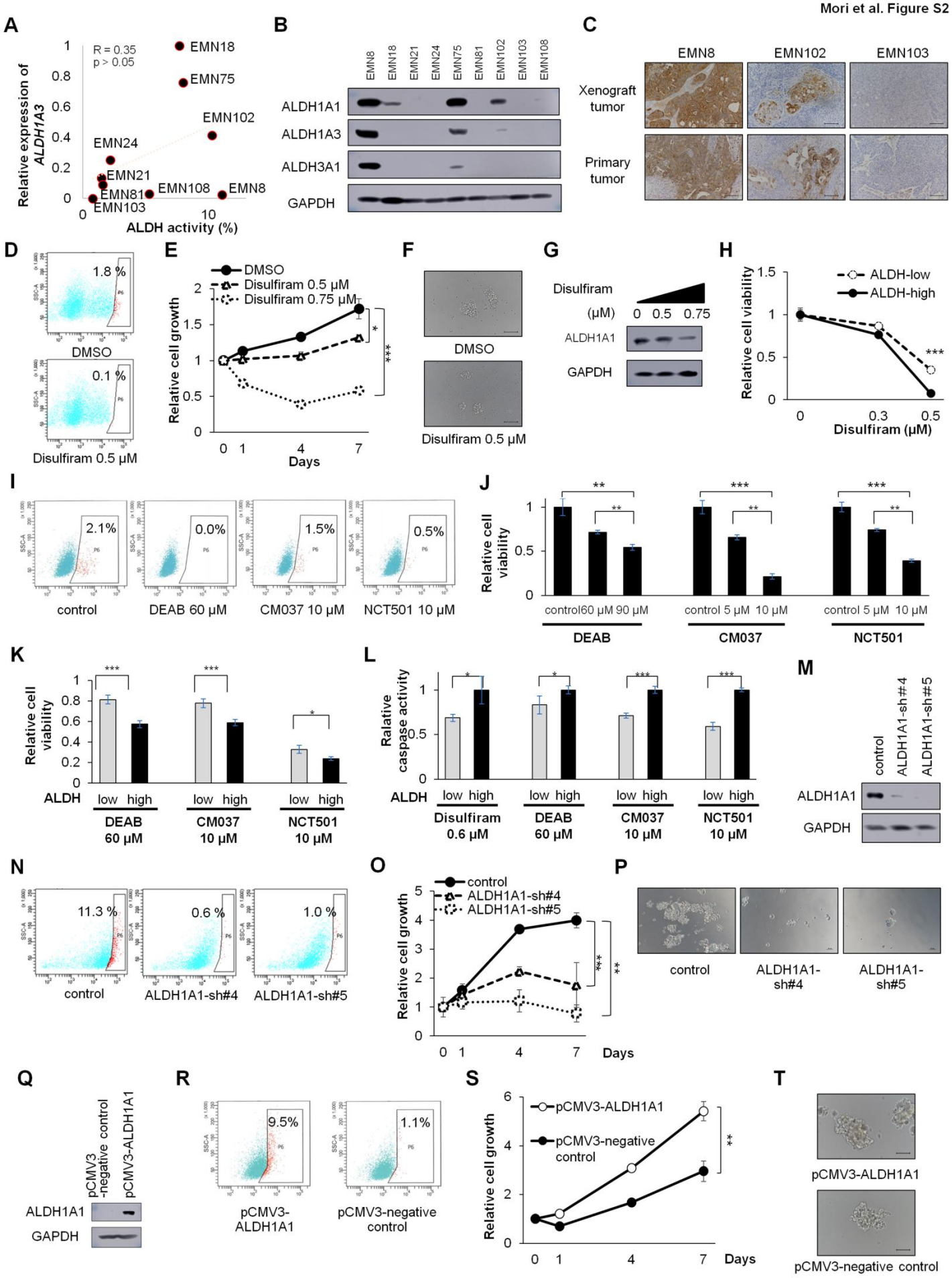
A
R = 0.35
p > 0.05
EMN18
EMN75
EMN102
EMN24
EMN21
EMN81
EMN108
EMN8
EMN103
Relative expression of ALDH1A3
ALDH activity (%)
B
EMN8
EMN18
EMN21
EMN24
EMN75
EMN81
EMN102
EMN103
EMN108
ALDH1A1
ALDH1A3
ALDH3A1
GAPDH
C
EMN8
EMN102
EMN103
Xenograft tumor
Primary tumor
D
1.8 %
DMSO
0.1 %
Disulfiram 0.5 μM
E
DMSO
Disulfiram 0.5 μM
Disulfiram 0.75 μM
Relative cell growth
Days
F
DMSO
Disulfiram 0.5 μM
G
Disulfiram (μM)
0 0.5 0.75
ALDH1A1
GAPDH
H
ALDH-low
ALDH-high
Relative cell viability
Disulfiram (μM)
I
2.1%
0.0%
1.5%
0.5%
control
DEAB 60 μM
CM037 10 μM
NCT501 10 μM
J
Relative cell viability
control 60 μM 90 μM
control 5 μM 10 μM
control 5 μM 10 μM
DEAB
CM037
NCT501
K
Relative cell viability
ALDH
low high
DEAB 60 μM
CM037 10 μM
NCT501 10 μM
L
Ralative caspase activity
ALDH
low high
Disulfiram 0.6 μM
DEAB 60 μM
CM037 10 μM
NCT501 10 μM
M
control
ALDH1A1-sh#4
ALDH1A1-sh#5
ALDH1A1
GAPDH
N
11.3 %
0.6 %
1.0 %
control
ALDH1A1-sh#4
ALDH1A1-sh#5
O
control
ALDH1A1-sh#4
ALDH1A1-sh#5
Relative cell growth
Days
P
control
ALDH1A1-sh#4
ALDH1A1-sh#5
Q
pCMV3-negative control
pCMV3-ALDH1A1
ALDH1A1
GAPDH
R
9.5%
1.1%
pCMV3-ALDH1A1
pCMV3-negative control
S
pCMV3-ALDH1A1
pCMV3-negative control
Relative cell growth
Days
T
pCMV3-ALDH1A1
pCMV3-negative control

Figure S2. Modification of ALDH affects the propagation and proliferation of spheroid cells. Related to Figure 2 and 3. A, Correlation between ALDH activity and *ALDH1A3* mRNA levels on culture day 10. B, Western blot analyses of spheroid cells on culture day 10. C, Immunostaining of ALDH1A1 in the indicated xenograft tumors and corresponding primary tumors. Scale bars, 100 μm. D, ALDH activity after treatment with DMSO or 0.5 μM disulfiram for 24 h (EMN81 cells). E, Time course of cell growth of the spheroids (EMN81 cells). n = 4 independent experiments, $p < 0.001$, Student's t-test. F, Bright-phase images of spheroids after disulfiram treatment for 7 days (EMN81 cells). Scale bars, 100 μm. G, Western blot analyses of spheroids after treatment with the indicated amounts of disulfiram for 24 h (EMN81 cells). H, Responses of ALDH-high and ALDH-low cells to different concentrations of disulfiram after incubation for 7 days (EMN81 cells). n = 4 independent experiments, $p < 0.001$, Student's t-test. I, ALDH activity after treatment with DMSO, 60 μM DEAB, 10 μM CM037, or 10 μM NCT501 for 24 h (EMN24 cells). J, Relative cell viability of spheroid cells after culture for 7 days with the indicated concentrations of ALDH inhibitor (EMN24 cells). n = 4 independent experiments, $p < 0.001$, Student's t-tests. K, Relative cell viability of ALDH-high and ALDH-low cells to ALDH inhibitor after incubation for 7 days (EMN24 cells). n = 4 independent experiments, Student's t-test. L, Relative caspase activity of ALDH-high and ALDH-low cells to ALDH inhibitor after incubation for 7 days (EMN24 cells). Student's t-tests. n = 4 independent experiments, Student's t-test. M, Western blot analyses after infection with the indicated lentiviruses (EMN8 cells). N, ALDH activity after ALDEFLUOR staining (EMN8 cells). O, Time course of proliferation of infected cells (EMN8 cells). n = 4 independent experiments, $p < 0.001$, Student's t-test. P, Bright-phase images of infected cells (EMN8 cells). Scale bars, 100 μm. Q, Western blot analyses of the spheroids after infection with the indicated lentiviruses (EMN21 cells). R, ALDH activity of the infected cells after ALDEFLUOR staining (EMN21 cells). S, Time course of proliferation of infected cells (EMN21 cells). n = 4 independent experiments, $p < 0.01$, Student's t-tests. T, Bright-phase images of the infected cells (EMN21 cells). Scale bars, 100 μm. *, $p < 0.05$; **, $p < 0.01$; ***, $p < 0.001$.

A

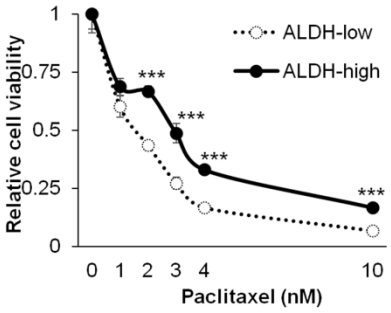

B

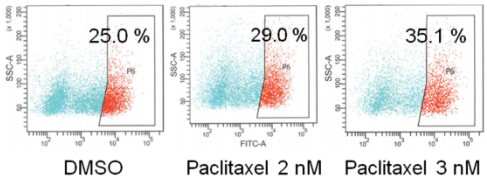

C

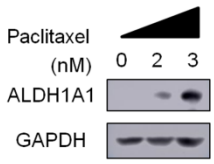

D

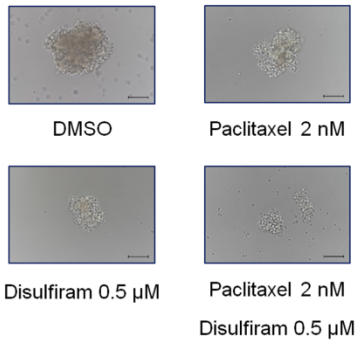

E

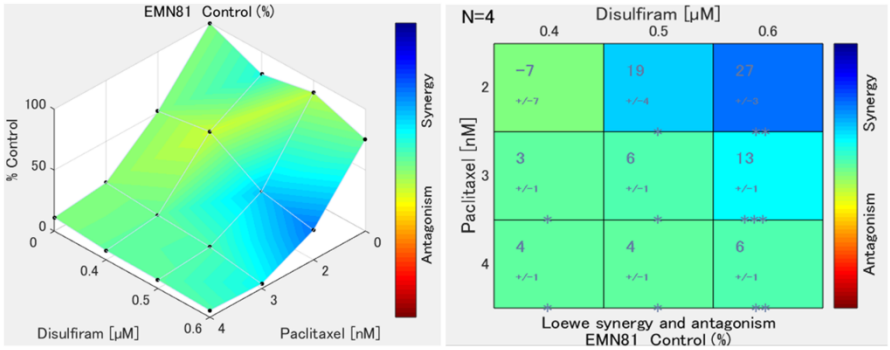

F

	Cell number							1/(stem cell frequency) (confidence intervals)
	64	32	16	8	4	2	1	
DMSO	6/12	3/12	2/12	1/12	1/12	1/12	0/24	89.6 (52.8-152)
Disulfiram	3/12	1/12	1/12	0/12	0/12	0/12	0/24	282.9 (118.5-677)
Paclitaxel	4/12	3/12	2/12	0/12	1/12	0/12	0/24	133.5 (71.6-249)
Paclitaxel Disulfiram	2/12	1/12	1/12	0/12	0/12	0/12	0/24	362 (136.2-963)

* * *

G

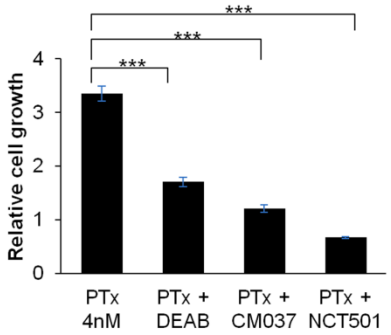

Figure S3. ALDH activity and expression are related to paclitaxel sensitivity of spheroid cells (EMN81 cells). Related to Figure 4. A, Responses of ALDH-high and ALDH-low cells to different concentrations of paclitaxel after incubation for 7 days. n = 4 independent experiments, $p < 0.001$, Student's t-tests. B, FACS analyses of ALDH activity in ALDH-high cells in the presence or absence of paclitaxel (7 days after the treatment). C, Western blot analyses of ALDH-high cells treated with paclitaxel for 7 days. D, Bright-phase images of spheroids after treatment with paclitaxel and disulfiram for 7 days. Scale bars, 100 μm. E, Relative cell viability of spheroid cells after culture for 7 days with the indicated concentrations of ALDH inhibitor and paclitaxel. Synergistic interaction was assessed with Combenefit software. n = 4 independent experiments. F, *in vitro* limiting dilution analysis for 14 days cultivation using spheroid cells exposed to disulfiram and/or paclitaxel *in vitro* for 7 days. G, Relative number of spheroid cells at 7 days after cultivation with paclitaxel and indicated ALDH inhibitor (EMN24 cells). n = 4 independent experiments, $p < 0.001$, Student's t-tests. *, $p < 0.05$; ***, $p < 0.001$.

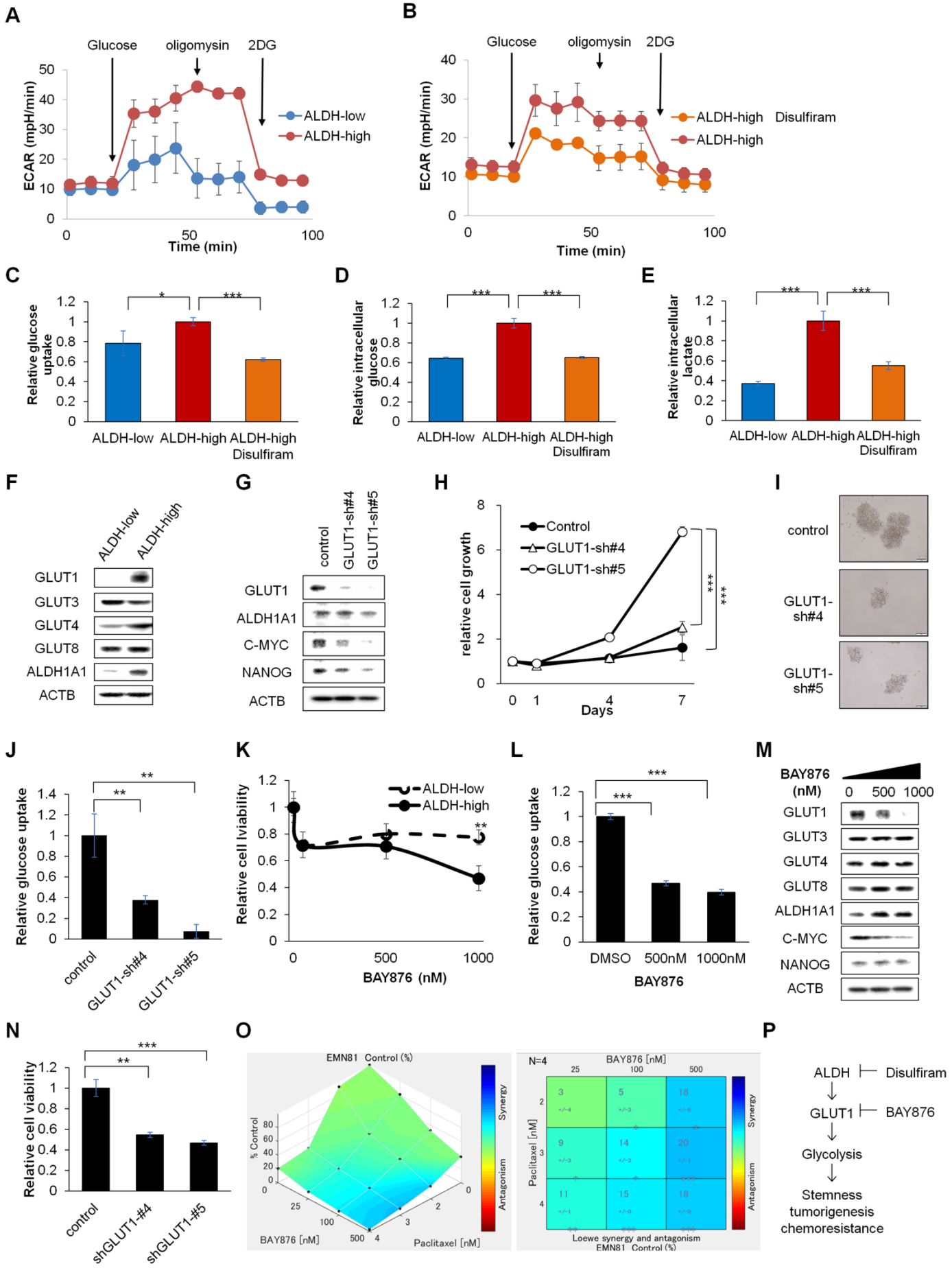
A
Glucose
oligomysin
2DG
ECAR (mpH/min)
Time (min)
ALDH-low
ALDH-high
B
Glucose
oligomysin
2DG
ECAR (mpH/min)
Time (min)
ALDH-high Disulfiram
ALDH-high
C
Relative glucose uptake
ALDH-low
ALDH-high
ALDH-high Disulfiram
D
Relative intracellular glucose
ALDH-low
ALDH-high
ALDH-high Disulfiram
E
Relative intracellular lactate
ALDH-low
ALDH-high
ALDH-high Disulfiram
F
ALDH-low
ALDH-high
GLUT1
GLUT3
GLUT4
GLUT8
ALDH1A1
ACTB
G
control
GLUT1-sh#4
GLUT1-sh#5
GLUT1
ALDH1A1
C-MYC
NANOG
ACTB
H
Control
GLUT1-sh#4
GLUT1-sh#5
relative cell growth
Days
I
control
GLUT1-sh#4
GLUT1-sh#5
J
Relative glucose uptake
control
GLUT1-sh#4
GLUT1-sh#5
K
ALDH-low
ALDH-high
Relative cell lviability
BAY876 (nM)
L
Relative glucose uptake
DMSO
500nM
1000nM
BAY876
M
BAY876 (nM)
0
500
1000
GLUT1
GLUT3
GLUT4
GLUT8
ALDH1A1
C-MYC
NANOG
ACTB
N
Relative cell viability
control
shGLUT1-#4
shGLUT1-#5
O
EMN81 Control (%)
% Control
BAY876 [nM]
Paclitaxel [nM]
Synergy
Antagonism
N=4
BAY876 [nM]
Paclitaxel [nM]
Loewe synergy and antagonism
EMN81 Control (%)
P
ALDH
Disulfiram
GLUT1
BAY876
Glycolysis
Stemness
tumorigenesis
chemoresistance

Figure S4. Combination therapy with paclitaxel and the GLUT1 inhibitor synergistically inhibits endometrial cancer cell progression (EMN81 cells). Related to Figure 6 and 7.

A-B, Time course of ECAR of spheroid cells with the indicated stimulation. The differences between ALDH-high and ALDH-low cells (A), and between ALDH-high cells with vehicle or disulfiram treatment (B). n = 4 independent experiments. C-E, Relative glucose uptake (C), intracellular glucose (D), and lactate level (E) of ALDH-low cells, ALDH-high cells, and ALDH-high cells treated with disulfiram. n = 4 independent experiments, $p < 0.01$, Student's t-test. F-G, Western blot analyses of ALDH-high and ALDH-low cells (F), and after infection with the indicated lentiviruses (G). H, Time course of the proliferation of the infected cells. n = 4 independent experiments, $p < 0.01$, Student's t-test. I, Bright-phase images of the infected cells. Scale bars, 100 μm. J, Relative glucose uptake of spheroid cells of the infected cells. n = 4 independent experiments, $p < 0.01$, Student's t-test. K-L, Relative cell viability (K) and glucose uptake (L) of spheroid cells after culture for 7 days with the indicated concentration of BAY876. n = 4 independent experiments, $p < 0.01$, Student's t-test. M, Western blot analyses of cells after exposure to the indicated concentration of BAY876. N, Relative cell viability of spheroid cells after culture for 7 days with 2 nM paclitaxel. n = 4 independent experiments, Student's t-test. O, Relative cell viability of spheroid cells with the indicated concentrations of BAY876 and paclitaxel *in vitro*. Synergistic interaction was assessed with Combenefit software. n = 4 independent experiments. P, A model of regulation of endometrial cancer stemness by ALDH and glycolysis. *, $p < 0.05$; **, $p < 0.01$; ***, $p < 0.001$.

Supplementary Table Legends

Table S1. Clinical data on endometrial cancer from which spheroid cells were obtained. Clinical stage was assigned according to the International Federation of Gynecology and Obstetrics (FIGO) staging system.

Table S2. Gene list of NCC oncopanel v4. Related to Figure 1 and Figure S1.

Table S3. The association between ALDH1A1 expression status and clinicopathological factors for 223 patients with early-stage and 35 patients with advanced-stage endometrial endometrioid cancer. Related to Figure 6.

Table S4. Association of ALDH1A1 expression with overall survival and progression-free survival in univariate analyses (35 cases of advanced disease). Related to Figure 6.

Table S5. Association of ALDH1A1 expression with overall survival and progression-free survival in multivariate analyses (35 cases of advanced disease). Related to Figure 6.

Table S6. List of antibodies used in this study

Supplemental Experimental Procedures

Tumor-derived spheroid culture

Endometrial cancer tissues were obtained from patients with primary endometrial cancer within 30 min of surgical excision. Tumor samples were placed on ice in phosphate-buffered saline (PBS) and transported to the laboratory. The samples were washed with PBS and mechanically cut into small pieces using a scalpel, followed by dissociation with 150 U/mL collagenase plus 50 U/mL hyaluronidase (Stemcell Technologies, Vancouver, BC, Canada) for 2 h at 37 °C. Dissociated cells were sequentially filtered through 100- and 70-μm cell strainers (BD Falcon). Collected cells were isolated through density gradient centrifugal purification in PBS containing Histodenz (Sigma, MO, USA). After lysis of red blood cells with ACK Lysing Buffer (Gibco), the remaining cells were grown on ultra-low-attachment culture dishes (Corning, NY, USA) in STEMPRO hESC SFM (Gibco) supplemented with 8 ng/mL basic fibroblast growth factor (Invitrogen, Carlsbad, CA, USA) and penicillin/streptomycin (37 °C, 5% CO_2). All dissociated cells from clinical samples formed sphere-like structures within 1 week. These spheroid cells grew stably *in vitro* after 1–6 months from the initial culture and continued to expand for more than 1 year. For serial passaging, spheroid cells were dissociated with Accumax (Innovative Cell Technologies) once every 14 days. For *in vitro* differentiation experiment, cells were cultivated with 10% FBS on standard attachment culture condition for 7 days.

Animal experiments

For drug efficacy studies, the mice were randomized into different groups. Disulfiram (40 mg/kg/day) and BAY876 (3.0 mg/kg/day) was administered five times/week, and paclitaxel (10 mg/kg/day) was administered three times/week, after injection of 1×10^5 spheroid cells. Mice were monitored every 3–4 days until 3–5 weeks after cell transplantation.

Targeted sequencing analysis

Genomic DNA samples were extracted from patient-derived frozen tumor tissues and spheroid cells. For targeted sequencing analysis, a SureSelect NCC Oncopanel v4 (Agilent Technologies) capturing all coding exons of 114 genes and translocated introns of 12 genes was used (Table S3). Sequencing libraries were constructed with a SureSelectXT Reagents Kit (Agilent Technologies) (Asano et al., 2017). Paired-end sequencing (2 x 150 bp) was performed on NextSeq 500 (Illumina, San Diego, CA, USA). Mutations (single-nucleotide variations and short insertions and deletions), gene amplifications, and gene fusions were detected using the cisCall (Clinical Sequence Call) system (Kato et al., 2018).

Gene set enrichment analysis (GSEA)

Microarray analyses were performed using Agilent Whole Human Genome 8 × 60 K oligo microarrays. Microarray data were accessible through the Gene Expression Omnibus database (accession number: GSE123530). Gene set enrichment analysis was performed using gene set collection version 6.2 from the Molecular Signatures Database (Subramanian et al., 2005, Mootha et al., 2003).

Flow cytometry analyses

Dissociated single spheroid cells were filtered, incubated with 7-AAD (BD Pharmingen) for exclusion of nonviable cells, and used for ALDEFLUOR assays (Stem Cell Technologies) or staining with antibody conjugated with phycoerythrin (Table S4). Xenograft tumors were enzymatically dissociated, and cancer cells were purified using a Mouse Cell Depletion Kit (Miltenyi Biotec). Samples were analyzed and sorted using a FACS Aria II Cell Sorter (BD Biosciences).

Cell-based assay

Cell viability was quantified by using CellTiter-Glo Luminescent Cell Viability Assays (Promega, Madison, WI, USA), and caspase-3/7 activity was quantified by using Caspase-Glo 3/7 (Promega) according to the manufacturer's instructions. The intensity of luminescence was measured using a FLUOROSCAN instrument (Thermo Scientific). After combination treatment exposure for 7 days (paclitaxel and disulfiram or BAY876) cell viability was quantified using CellTiter-Glo Luminescent Cell Viability Assays (Promega), synergistic interaction was assessed with Combenefit software tool (Di Veroli et al., 2016). All *in vitro* cell-based assays except stem cell frequency assay were performed in quadruplicate and expressed as mean ± SD.

Stem cell frequency assay

Stem cell frequency was calculated with the extreme limiting dilution analysis (ELDA) algorithm (Hu et al., 2009). For *in vitro* analysis, dissociated spheroid cells were seeded into at least 12 wells of the 96-well plate each different cell numbers. After 14 days cultivation, cell clusters > 50 μm in diameter were identified as spheres. To calculate the stem cell frequency after drug exposure, spheroid cells were cultivated with vehicle, paclitaxel, or disulfiram for 7 days. Subsequently, survival dissociated cells were

cultivated in standard cultivation condition for 14 days and counted spheres.

Immunohistochemical analyses

Primary or mouse xenograft tumors were fixed in neutral formalin, embedded in paraffin, and used for staining with hematoxylin and eosin (H&E). For immunostaining, the sections were stained following standard IHC methods, as previously described (Ishiguro et al., 2016), with primary antibodies (Table S4) and biotinylated secondary antibodies (Vector Laboratories, Burlingame, CA, USA), followed by incubation with ABC reagent (Dako) and 3,3'-diaminobenzidine (Sigma).

For staining evaluation, three randomized areas of samples were evaluated by two observers. The extent of staining was visually evaluated on a scale of four levels ("0" indicating no staining to "3" indicating strong staining). Samples with weak, moderate, or strong ALDH1A1 staining (staining intensity scored as 1, 2, or 3, respectively) in at least 10% of cancer cells were regarded as IHC-ALDH-positive, and samples without staining (staining intensity scored as 0) and less than 10% staining of cells were regarded as IHC-ALDH-negative. For evaluating GLUT1 staining, samples with strong staining in at least 50% of cancer cells as IHC-GLUT1-high, and the others were regarded as IHC-GLUT1-low.

Immunocytochemical analyses

Spheroid cells dissociated with Accumax were attached to glass slides using a gelatinizing agent (Smear Gell, Geno Staff), fixed in 4% paraformaldehyde in PBS for 15 min, washed with 1× PBS, permeabilized with PBS/0.1% Triton X-100 for 5 min at 4 °C, and blocked with PBS containing 3% bovine serum albumin. The fixed cells were then used for immunostaining with primary antibodies (Table S4) and secondary Alexa-594 donkey anti-goat antibodies (Abcam), followed by counterstaining with 4',6 diamidino-2-phenylindole.

Quantitative real-time reverse transcription polymerase chain reaction (qRT-PCR) analyses

RNA was isolated from cells with an miRNeasy Micro kit (Qiagen, Valencia, CA, USA), and cDNA was synthesized from total RNA using a PrimeScript First Strand cDNA Synthesis Kit (Takara, Shiga, Japan). Gene expression levels were measured by performing TaqMan gene expression assays (Applied Biosystems/Life Technologies, Carlsbad, CA, USA) with an ALDH1A1 (Hs00946916_m1) or ALDH1A3 (Hs00167476_m1) primer/probe set according to the manufacturer's instructions. Glyceraldehyde 3-phosphate

dehydrogenase was used to calculate delta Ct values for genes.

ECAR measurement

Extracellular acidification rate (ECAR) was measured by the Seahorse XFe-24 Extracellular Flux Analyzer using the Glycolysis Stress Test Kit following the manufacturer's protocol. Cells were seeded at 4×10^5 /well for 24 well plates coated by Poly-D-lysine hydrobromide and centrifuged to attach to the plate. Basal ECAR was measured in glucose-free medium and cells were subjected to sequential injections of glucose 10mM, oligomycin 1.0μM, and 2-deoxyglucose 50mM into the medium.

Metabolic assay

Intracellular Glucose levels and Lactate levels were measured with Glucose-Glo-Assay and Lactate-Glo-Assay (Promega). Glucose uptake of cells was measured with Glucose Uptake-Glo (Promega). All of the measured values were corrected by the number of cells.

Supplemental References

Asano, N., Yoshida, A., Mitani, S., Kobayashi, E., Shiotani, B., Komiyama, M., Fujimoto, H., Chuman, H., Morioka, H., Matsumoto, M., et al. (2017) Frequent amplification of receptor tyrosine kinase genes in welldifferentiated/ dedifferentiated liposarcoma. Oncotarget. 8, 12941-12952.

Di Veroli, G. Y., Fornari, C., Wang, D., Mollard, S., Bramhall, J. L., Richards, F. M. & Jodrell, D. I. (2016) Combenefit: an interactive platform for the analysis and visualization of drug combinations. Bioinformatics. 32, 2866-2868.

Hu, Y. & Smyth, G. K. (2009) ELDA: extreme limiting dilution analysis for comparing depleted and enriched populations in stem cell and other assays. J Immunol Methods. 347, 70-78.

Ishiguro, T., Sato, A., Ohata, H., Ikarashi, Y., Takahashi, R. U., Ochiya, T., Yoshida, M., Tsuda, H., Onda, T., Kato, T., et al. (2016) Establishment and characterization of an in vitro model of ovarian cancer stem-like cells with an enhanced proliferative capacity. Cancer Res. 76, 150-160.

Kato, M., Nakamura, H., Nagai, M., Kubo, T., Elzawahry, A., Totoki, Y., Tanabe, Y., Furukawa, E., Miyamoto, J., Sakamoto, H., et al. (2018) A computational tool to detect DNA alterations tailored to formalin-fixed paraffin-embedded samples in cancer clinical sequencing. Genome Med. 10, 44.

Mootha, V. K., Lindgren, C. M., Eriksson, K. F., Subramanian, A., Sihag, S., Lehar, J., Puigserver, P., Carlsson, E., Ridderstrale, M.,

Laurila, E., et al. (2003) PGC-1alpha-responsive genes involved in oxidative phosphorylation are coordinately downregulated in human diabetes. Nat Genet. 34, 267-273.

Subramanian, A., Tamayo, P., Mootha, V. K., Mukherjee, S., Ebert, B. L., Gillette, M. A., Paulovich, A., Pomeroy, S. L., Golub, T. R., Lander, E. S., et al. (2005) Gene set enrichment analysis: a knowledge-based approach for interpreting genome-wide expression profiles. Proc Natl Acad Sci U S A. 102, 15545-15550.